

1      Are historical stage records useful to decrease the uncertainty of flood  
2                          frequency analysis ? A 200-year long case study

3      Mathieu LUCAS <sup>\*1</sup>, Benjamin RENARD<sup>2</sup>, Jérôme LE COZ<sup>1</sup>, Michel LANG<sup>1</sup>, Antoine BARD<sup>3</sup>,  
4                          and Gilles PIERREFEU<sup>4</sup>

5                          <sup>1</sup>INRAE, UR RIVERLY, Villeurbanne, France

6                          <sup>2</sup>INRAE, UR RECOVER, Aix-en-Provence, France

7                          <sup>3</sup>ESDB, Briançon

8                          <sup>4</sup>CNR, Lyon

9                          June 12, 2023

10                         **Abstract**

11      Flood frequency analysis (FFA), a widely used method to estimate flood hazard, is affected by several  
12      sources of uncertainty. Extending flood samples by reanalyzing historical continuous stage records has the  
13      potential to reduce sampling uncertainty, but the historical flood discharges derived from this reanalysis  
14      are generally affected by large uncertainties. This paper explores whether historical stage records improve  
15      design flood estimates through a chain of uncertainty estimation methods for FFA. Uncertainties are  
16      estimated and propagated from stage and rating curves to design flood estimates using Monte Carlo  
17      procedures. The role of both streamflow and sampling uncertainties in design flood estimation is examined.  
18      This procedure is applied to the 205-year long continuous stage series of the Rhône River at Beaucaire,  
19      France ( $95\ 590\ km^2$ ). The estimated streamflow 95% uncertainty varies from 30% (XIX<sup>th</sup> Century) to 5%  
20      (1967-2020). The total uncertainty of design flood is significantly reduced when the length of the series  
21      increases from 20 to 100 years due to sampling uncertainty reduction. However, the total uncertainty  
22      remains stable beyond this sample size: this is because large uncertainties affecting the XIX<sup>th</sup> Century  
23      flood discharges compensate for the reduction in sampling uncertainty. Enlarging the sample size to two  
24      centuries leads to including the two largest known floods in 1840 and 1856. In turn, this induces a 15%  
25      increase of the 1000-year flood estimates ~~a minor difference considering the associated uncertainty~~.

26      **Keywords:** Flood frequency analysis, Historical stage records, Uncertainty propagation, Streamflow  
27      uncertainty, Sampling uncertainty

---

\*Corresponding author at: INRAE, 5 Rue de la Doua, 69100 VILLEURBANNE, FRANCE.

E-mail adress: mathieu.lucas@inrae.fr (M. Lucas).

28 **1 Introduction**

29 Flood frequency analysis (FFA) is a widely used method to estimate flood hazard. It allows linking the  
30 magnitude of a flood to its probability of occurrence (Hamed and Ramachandra Rao (2019); Jain and Singh  
31 (2019)). Flood estimates for various exceedance probabilities or, equivalently, return periods, are commonly  
32 used for population safety policies, land use planning, as well as industrial safety. The standard FFA  
33 approach is to estimate a distribution using a sample of flood peaks, typically defined as annual maximum  
34 discharges or discharges over a given threshold. This distribution may be extrapolated to reach the desired  
35 flood quantile that typically corresponds to a 100 or 1000-year return period (see Le Delliou, 2014 for dam  
36 safety regulations in France).

37 This FFA approach is affected by various sources of uncertainty. First, the hydrological data used to  
38 estimate the FFA distribution is uncertain. Indeed, streamflow time series are generally derived from stage  
39 time series through rating curve models (Rantz, 1982). This procedure includes ~~measurement (gaugings  
40 and stage) and model (rating curve) errors~~ three types of errors on hydrological data: stage measurement;  
41 discharge measurement (gaugings); stage-discharge model (rating curve). Moreover, the estimated FFA  
42 distribution is also affected by sampling uncertainty resulting from the limited size of available streamflow  
43 data (Kjeldsen et al., 2011). Considering the importance of decisions relying on FFA results, a consis-  
44 tent treatment of uncertainty all over the data processing chain (including both streamflow and sampling  
45 uncertainties) is essential but is usually not performed.

46 Streamflow series are affected by several sources of uncertainty as described by McMillan et al. (2012).  
47 First, a large number of stage error sources are identified in the literature (Van Der Made (1982); Petersen-  
48 Øverleir and Reitan (2005); McMillan et al. (2012); Horner et al. (2018)), such as staff gauge reading,  
49 levelling of the staff gauge, or stage sensor calibration. The frequency of measurement may also induce time  
50 interpolation errors. With modern automatic gauges, stage is generally measured with a time step small  
51 enough (e.g. between 15 min and 1 hour) to get negligible time interpolation errors. However, before the rise  
52 of automatic gauges, measurements were made by operators who read the staff gauge less frequently (e.g.  
53 once or a few times per day), thus possibly missing the flood peak. This issue is particularly critical when  
54 old stage series are used. Hamilton and Moore (2012) and Kuentz et al. (2014) estimated the measurement  
55 frequency error by sub-sampling recent, sub-hourly measurements. They calculated the difference between  
56 the variable of interest (such as the daily maximum stage) derived from scarce data, and the same variable  
57 derived from high-frequency measurements. Kuentz et al. (2014) applied the (monthly-averaged) calculated  
58 bias to correct old stage series. This correction aimed at taking into account the error due to the daily

59 variability caused by snow melt. However, this type of correction has never been applied to peak stage  
60 correction during floods, especially in the case of long stage series.

61 Rating curve uncertainty is also a major issue when dealing with streamflow series. Transforming stage  
62 into discharge requires calibration data (gaugings) to establish the stage-discharge relationship. Note that  
63 the term "gauging" corresponds in this paper (and in the French practice) to the sporadic measurement  
64 of the stage-discharge couple, which can correspond to the term "discharge measurement" in the British  
65 or American practice. Gaugings uncertainty depends on the measurement method (Le Coz et al. (2014a);  
66 Puechberty et al. (2017)). Moreover, the rating curve is also affected by uncertainties coming from the  
67 imperfection of the chosen model to represent the actual hydraulic configuration, and from parameter  
68 estimation. Many methods have been proposed to quantify these uncertainties (Petersen-Øverleir et al.  
69 (2009); Juston et al. (2014); Le Coz et al. (2014b); Morlot et al. (2014); Coxon et al. (2015); McMillan and  
70 Westerberg (2015); Mansanarez et al. (2019b)). A comparison of several of these methods has been recently  
71 proposed by Kiang et al. (2018). Another important issue affecting streamflow data accuracy is rating  
72 changes. The stage-discharge relationship is frequently affected by changes caused by various factors, either  
73 natural or anthropic, for instance: bed geometry evolution during floods or river works, aquatic vegetation  
74 growth and decay, ice cover... A regular monitoring through gaugings is essential to detect those changes  
75 (Ibbitt and Pearson, 1987) that can be transient or sudden. Several methods have been proposed to deal with  
76 rating changes: estimating rating curves on moving temporal windows (Westerberg et al. (2011); Guerrero et  
77 al. (2012)), computing as many rating curves as there are gaugings (Morlot et al., 2014), exploring changes  
78 in the annual minimum stages (Lapuszek and Lenar-Matyas, 2015), selecting the 0.5-year return period  
79 discharge as a threshold for rating changes (McMillan et al., 2010). More recently, Darienzo et al. (2021)  
80 proposed a method based on a recursive segmentation procedure, accounting for both gaugings and rating  
81 curve uncertainties. This method has a particular interest when dealing with old and uncertain gaugings.  
82 Following the detection of rating shifts, rating curves should be estimated for each stable period. This  
83 task may not be straightforward, as the number of gaugings available within a stable period is not always  
84 sufficient to properly estimate the stage-discharge relationship for the whole discharge range. A common  
85 way to address this problem is to artificially repeat some gaugings from other stable periods A common way  
86 to address the lack of gaugings (in particular flood gaugings) within some of the stable periods is to use  
87 gaugings from the other stable periods (McMillan et al. (2012); Puechberty et al. (2017)). Mansanarez et al.  
88 (2019a) proposed an alternative approach to deal with this issue. They developed a stage-period-discharge  
89 (SPD) model where rating curve parameters may vary across periods, while others are supposed constant.  
90 This method has the advantage of transferring information between periods to improve the rating curve  
91 estimation, even when few gaugings are available.

92 Estimating sampling uncertainty in FFA is a well-established approach. Whatever the chosen distribution  
93 and estimation method, standard statistical procedures are available (Coles, 2001). However, these standard  
94 procedures only quantify sampling uncertainty, they do not consider data uncertainty. The literature review  
95 proposed in the previous paragraphs shows that methods for quantifying individual sources of uncertainty  
96 (stage, rating curve and FFA distribution estimation) are available. However, the way these multiple un-  
97 certainties propagate through the FFA analysis chain has been less thoroughly studied. A few solutions  
98 have emerged to propagate uncertainties in stage time series through uncertain rating curves (Dymond and  
99 Christian (1982); Herschy (1998); Petersen-Øverleir and Reitan (2005)), but they assume independent stage  
100 errors and therefore neglect systematic errors. Horner et al. (2018) proposed a method for the propagation  
101 of both sources of stage uncertainty through uncertain rating curves. Therefore, it is possible to distinguish  
102 the effects of independent and systematic stage errors on streamflow uncertainty. Petersen-Øverleir and  
103 Reitan (2009), Steinbakk et al. (2016), and Vieira et al. (2022) performed an integrated analysis in which  
104 both rating curve parameters and flood frequency distribution are estimated. These studies highlighted  
105 the importance of considering rating curve uncertainty for design flood estimations and concluded that,  
106 under some conditions, accounting for rating curve uncertainty may notably widen the uncertainty intervals  
107 around flood quantiles. However, these studies did not consider stage measurement and time interpolation  
108 errors nor rating changes, which may constitute a major source of uncertainty for streamflow data. This  
109 is particularly the case when dealing with long streamflow series for which stage uncertainty is large and  
110 variable through time, and rating changes may have been missed. Their consideration in a flood frequency  
111 framework is therefore not avoidable.

112 The following questions will be considered in this paper:

- 113 1. How to make the most of historical hydrometric (based on stage records) data in flood frequency  
114 analysis while accounting for multiple and variable uncertainties at each step of the procedure ?
- 115 2. What is the contribution of each source of uncertainty to the flood quantile uncertainty when historical  
116 data are taken into account ?
- 117 3. To what extent does enlarging streamflow samples by adding increasingly uncertain historical data  
118 improve flood quantiles estimation ? How are the relative contributions of sampling and streamflow  
119 uncertainties evolving with sample size ?

120 Note that the "historical data" term used in this paper refers to the use of ~~ancient but regularly measured~~  
121 stage series ~~old but continuously measured stage series~~, as opposed to sporadic flood marks, prior to regular  
122 stage measurements.

123 This paper illustrates the chained application of methods to quantify and propagate uncertainty from  
124 stage records (and their limited time resolution) and stage-discharge rating curves to the estimation of  
125 **design flood distribution with uncertainties**. While most of these methods already exist, a key novelty  
126 of this work is their combination in a consistent framework (Figure 1) to provide an end-to-end evaluation  
127 of the uncertainty affecting FFA estimates. An original method to quantify the stage uncertainty stemming  
128 from infrequent readings is also proposed.

129 The paper is organized as follows. First, the methodology for establishing uncertain streamflow series  
130 in a century-long context is presented. It goes through the detection of rating shifts (section 2.1), the  
131 estimation of rating curves (section 2.2), and the estimation (section 2.3) and propagation (section 2.4) of  
132 stage errors. Then, an approach to propagate streamflow uncertainty through the estimation of extreme  
133 flood quantiles is proposed (section 2.5). This procedure is applied to the Beaucaire gauge on the Rhône  
134 River (section 3), ~~which official design flood estimates is based on which previous official FFA only used a 80-~~  
135 year long discharge series (Rigaudière et al., 2000). ~~In France, the official design flood for flood risk mapping~~  
136 ~~is based on the “largest known flood” or the Q100 flood (AEP=0.01) if the latter is greater. Uncertainty is~~  
137 ~~not taken into account in the official rules.~~ The recent works of Pichard et al. (2017) and Bard and Lang  
138 (2018) provided a continuous stage series from 1816 to the present time, which makes it the ideal case study  
139 for demonstrating this procedure. The results of this application are presented in section 4, and they are  
140 discussed in section 5, where avenues for improvements are proposed.

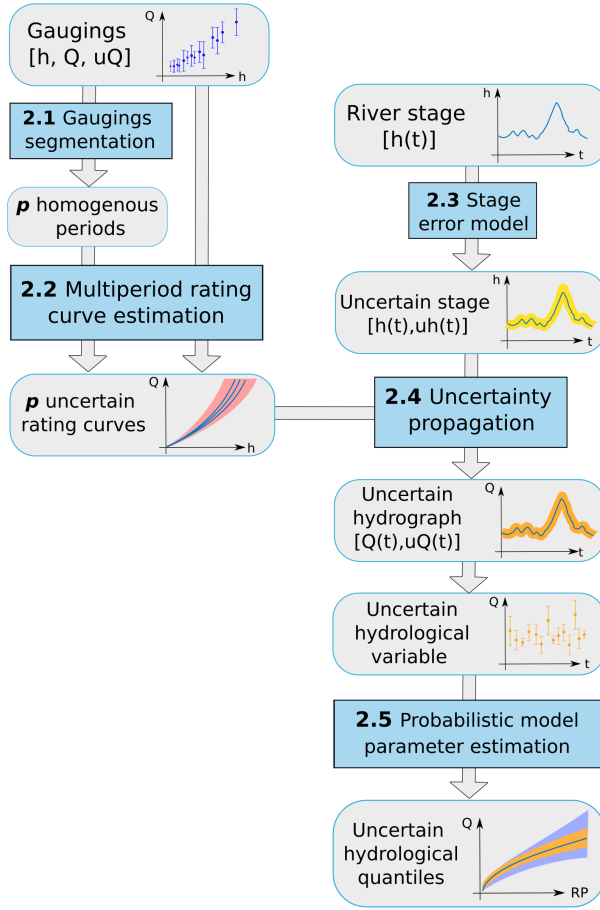


Figure 1: Block diagram of the uncertainty propagation procedure. Grey blocks represent data, blue blocks stand for analysis methods/models that correspond to the sub-sections of this article.  $h$  is the water stage,  $uh$  the stage uncertainty,  $Q$  the discharge,  $uQ$  the discharge uncertainty,  $t$  is the time and  $RP$  the return period of flood quantiles.

## <sup>141</sup> 2 Uncertainty propagation chain for flood frequency analysis

### <sup>142</sup> 2.1 Rating shifts detection

<sup>143</sup> The stage-discharge relationship is sensitive to sudden changes caused by morphogenic floods or other causes  
<sup>144</sup> affecting the flow characteristics. Relying on residuals between the gaugings and the rating curve is the most  
<sup>145</sup> common approach to monitor the stability of this relationship over time. The method proposed by Darienzo  
<sup>146</sup> et al. (2021) is used in this work and can be summarized as follows. First, a baseline rating curve is estimated  
<sup>147</sup> from the whole gaugings dataset. The residuals between gaugings and the rating curve are determined, and a  
<sup>148</sup> statistical segmentation procedure is applied to them. This procedure accounts for the residuals uncertainty,  
<sup>149</sup> coming from both the gaugings uncertainty and the rating curve uncertainty. The optimal number of **stable**  
<sup>150</sup> sub-periods is determined based on the Bayesian Information criterion (BIC). Then, the same steps are  
<sup>151</sup> applied recursively to each sub-period. The recursive procedure is stopped when the BIC indicates that a  
<sup>152</sup> single period is optimal for all sub-periods. The results are not only the dates of the rating shifts but the  
<sup>153</sup> posterior probability density functions (pdf) of change point times. This allows affecting the shift time to the

time of the maximum stage included in the posterior 95% credibility interval. Prior knowledge is provided on the mean of the residuals in each sub-period. The maximum number of segments at each iteration also needs to be specified. All technical details can be found in Darienzo et al. (2021).

## 2.2 Multi-period rating curves estimation: stage-period-discharge model

Once the **stable** periods have been identified, the next step is to estimate the rating curves. Mansanarez et al. (2019a) developed a stage-period-discharge (SPD) model "based on the physical interpretation of changes in the stage-discharge relation across a series of stability periods". The SPD model is based on the BaRatin model (Le Coz et al., 2014b).

BaRatin uses the Bayesian paradigm to estimate the parameters of the rating curve equation, a combination of power equations:  $Q = a(h - b)^c$ , where  $Q$  is the discharge,  $h$  is the stage,  $b$  is an offset (corresponding to the cease-to-flow stage), and  $a$  and  $c$  are the coefficient and the exponent of the power function. The rating curve equation is deduced from a hydraulic analysis of the gauging station, aimed at identifying the main hydraulic controls governing the stage-discharge relation. The multiple controls can be activated successively or simultaneously. Bayesian inference allows deriving the posterior distribution of rating curve parameters by combining hydraulic information (priors for parameters of each hydraulic control) and information from gaugings with uncertainty (likelihood). Two sources of uncertainty are associated with the estimated rating curve. Parametric uncertainty reflects the uncertainty due to the rating curve parameters estimation because of the limited amount of gaugings and the gaugings uncertainty. Remnant uncertainty comes from the imperfection of the chosen rating curve model to represent the actual hydraulic configuration. The posterior distribution is explored using a Markov Chain Monte Carlo (MCMC) sampler, leading to  $m$  realizations of the rating curve parameter vector representing parametric uncertainty. We refer the reader to Le Coz et al. (2014b) for a more thorough description.

The SPD model estimates the rating curves of each **stable** period based on the same principle by considering that some parameters vary in time, while others remain constant throughout the **stable** periods. An important step is the identification of those varying parameters based on an hydraulic analysis of the site. Generally, channel depths and/or widths are suspected to change. A distinction is made between "local changes" affecting the lowest control only (for instance the movement of the controlling riffle) and "overall changes" affecting several controls at the same time (for instance, the scouring or filling of the main channel, affecting the offsets of both the low-flow controlling riffle and the main channel itself). Prior specification for varying parameters can be based on the analysis of the yearly lowest stages, which provide information on the evolution of riverbed elevation, as described by Lapuszek and Lenar-Matyas (2015). See Mansanarez

185 et al. (2019a) for a detailed description of prior specification for time-varying rating curves. Specific investigation is needed to correctly account for past flood surveys of the cross section, as complex filling/erosion  
186 process may have been encountered during a flood with morphogenic changes.

## 188 2.3 Stage uncertainties

189 Many sources of error having distinct statistical properties can affect stage measurements, as described in  
190 Horner et al. (2018). Five different sources of error ( $\delta_{1,\dots,5}$ ) affecting stage measurements are considered.  
191 Let  $h(t)$  be the measured maximum stage of a day  $t$ . The unknown true maximum stage  $\hbar(t)$  is assumed to  
192 be approximated by the following equation:

$$\hbar(t) = h(t) + \delta_1(t) + \delta_2(t) + \delta_3(t) + \delta_4(t) + \delta_5(t) \quad (1)$$

193 Staff gauge reading errors  $\delta_1 \sim \mathcal{N}(0, \sigma_1)$  originate from operators reading the gauge, where  $\sigma_1$  depends  
194 on the resolution of the graduations (usually 1 cm), and can be increased by waves, especially during floods  
195 (McMillan et al., 2012).

196 Nowadays, most stage measurements are done with automatic sensors of various types such as pressure  
197 sensors, floats, radars, and they require a calibration to link the water stage to the measured proxy (respec-  
198 tively the pressure of the water column, the height of a float, or the air draught). Two types of errors arise  
199 from this process: sensor errors  $\delta_2 \sim \mathcal{N}(0, \sigma_2)$ , where  $\sigma_2$  is usually estimated by the sensor manufacturer,  
200 and sensor calibration errors  $\delta_3 \sim \mathcal{N}(0, \sigma_3)$  that are related to the corrections made by operators when  
201 comparing the stage measured by the sensor to the actual stage at the staff gauge reference. An operator  
202 error at this step could affect the stage measurement until the next calibration. Sensor calibration error  $\delta_3$   
203 is hence assumed constant between two calibrations and can be represented by drawing a new random value  
204 at each operator intervention.

205 Datum errors  $\delta_4 \sim \mathcal{N}(0, \sigma_4)$  are related to changes in the datum reference elevation of the staff gauge zero  
206 value and possible discontinuity between successive gauges. Similarly to  $\delta_3$ , this error is constant between  
207 two gauge changes or datum reference measurements.

208 Measurement frequency errors  $\delta_5$  are related to the inadequacy of the frequency of measurement with  
209 respect to the rate of stage variations, leading to the true daily maximum occurring in between measurements.  
210 Unlike other types of stage errors, this error is hence necessarily positive, which calls for using a positive  
211 distribution such as the Exponential distribution. The parameters of this distribution can be estimated  
212 with data from the recent period, by analyzing the difference between the daily maximum stage derived

213 from the high-frequency sensor measurement and that from an infrequent fixed-time reading. Note that the  
214 frequency errors for hourly (or more frequent) measurements are considered negligible for large rivers with  
215 slow variations, such as the Rhône River at Beaucaire.

216 To sum up,  $\delta_1$ ,  $\delta_2$  and  $\delta_5$  errors are drawn at each measurement time step, while  $\delta_3$  and  $\delta_4$  errors are only  
217 drawn at specific calibration times. Errors  $\delta_1$  to  $\delta_4$  are assumed Gaussian with known standard deviations,  
218 while  $\delta_5$  is assumed Exponential with parameter estimated by subsampling recent measurements. For each  
219 error type, 500 realizations are drawn from their respective distribution. Applying eq. 1, the total stage  
220 uncertainty is therefore represented by 500 possible realizations of the stage  $h(t)$ .

## 221 2.4 Propagation of stage and rating curve uncertainties to streamflow time series

222 Stage realizations can be propagated through uncertain rating curves, following the approach described by  
223 Horner et al. (2018). Four cases are considered to estimate the contributions of the different sources of  
224 streamflow uncertainty:

- 225 • **Case 1: Maxpost streamflow.** Stage is taken as the median of the stage time series realizations.  
226 This unique stage time series is propagated through the maxpost (Maximum A Posteriori: obtained  
227 with parameters maximizing the posterior pdf) rating curve, resulting in a single discharge time series.
- 228 • **Case 2: Stage uncertainty.** The  $n=500$  possible stage time series are propagated through the  
229 maxpost rating curve. Thus,  $n$  discharge time series are obtained.
- 230 • **Case 3: Stage and parametric rating curve uncertainty.** The  $n=500$  realizations of stage time  
231 series are propagated through  $m$  rating curves, corresponding to the  $m$  MCMC-simulated parameter  
232 vectors described in section 2.2. This leads to  $n \times m$  discharge time series.
- 233 • **Case 4: Total streamflow uncertainty.** It is obtained by adding remnant rating curve uncertainty  
234 (as defined in section 2.2) to case 3. To achieve this,  $n \times m$  time series of remnant errors are sampled  
235 from their estimated distribution and added to the time series created for case 3.

## 236 2.5 Estimation of probabilistic model parameters and flood frequency analysis

237 The Generalized Extreme Value (GEV) distribution is commonly used to model annual maximum discharges  
238 (AMAX) (see Hamed and Ramachandra Rao (2019) or Jain and Singh (2019)). The vector  $\theta = (\mu, \sigma, \xi)$   
239 denotes the location, scale and shape parameters of the GEV distribution. The parameters can be estimated  
240 based on an independent and identically distributed (*iid*) sample of  $j$  annual maximum discharges  $(q_t)_{t=1,\dots,j}$ .  
241 Bayesian-MCMC estimation is used in this work, as described in Coles (2001). The posterior distribution

242 quantifies sampling uncertainty and can be represented by  $r$  MCMC-generated GEV parameter vectors  
243  $\Theta = (\theta_1, \dots, \theta_r)$ . The maxpost vector is noted  $\hat{\theta}$ .

244 As described in section 2.4, total streamflow uncertainty is represented by  $n \times m$  possible realizations of  
245 the streamflow, hence of the AMAX series  $(q_t^{(i)})_{i=1,\dots,n \times m; t=1,\dots,j}$ , that are subsampled to  $s=500$  realizations  
246 to reduce computation time. The estimated flood quantiles should consider both sampling and streamflow  
247 uncertainties. Similarly to Steinbakk et al. (2016), the aim is to estimate the contribution of each source to  
248 the total uncertainty. For this purpose, three cases can be considered:

249 • **Case 1: Maxpost quantiles.** The GEV distribution is estimated using the single AMAX series  
250  $\hat{\mathbf{q}} = (\hat{q}_t)_{t=1,\dots,j}$  derived from the maxpost streamflow series (case 1 in section 2.4). Flood quantiles are  
251 then computed using the maxpost GEV parameters  $\hat{\theta} = (\hat{\mu}, \hat{\sigma}, \hat{\xi})$ . In this case, both streamflow and  
252 sampling uncertainties are ignored.

253 • **Case 2: Streamflow uncertainty.** The GEV distribution is estimated for each possible AMAX  
254 realization:  $\mathbf{q}^{(i)} = (q_t^{(i)})_{t=1,\dots,j; i=1,\dots,s}$ . However, only the maxpost GEV parameters vector is retained  
255 for each realization. This results in  $s$  vectors of GEV parameters  $(\hat{\theta}^{(i)})_{i=1,\dots,s}$  that represent the effect  
256 of streamflow uncertainty of flood quantiles, ignoring sampling uncertainty.

257 • **Case 3: Total uncertainty.** Similarly to Case 2, the GEV distribution is estimated for each of the  
258  $s$  realizations of the AMAX series, but all the  $r$  MCMC-simulated GEV parameters are used, leading  
259 to  $s \times r$  vectors of GEV parameters  $(\theta_k^{(i)})_{k=1,\dots,r; i=1,\dots,s}$ . The result thus reflects both sampling and  
260 streamflow uncertainties.

### 261 3 Case study: The Rhône River at Beaucaire

#### 262 3.1 Site

263 The Rhône River at Beaucaire ( $95\ 590\ km^2$ ) is the lowest gauge of the Rhône River (Figure 2). It cap-  
264 tures all the complexity of the Rhône River hydrological regime, from the Alpine area to the oceanic and  
265 Mediterranean influences. The annual mean discharge is around  $1700\ m^3/s$  (Bard and Lang, 2018), and the  
266 maximum known discharge reached  $12\ 500\ m^3/s$  (May 1856, Lang and Coeur (2014)). The station lies in a  
267 flood sensitive area, as illustrated by the recent 2003 flood, resulting in 1.1 billion euros worth of damage  
268 (Lang and Coeur, 2014). The first stage measurements started in 1816, close to the bridge linking the cities  
269 of Beaucaire and Tarascon. This station is named "Pont de Beaucaire" (Kilometric point 267.6 from Lyon).  
270 It has been used until the construction of the Vallabregues hydroelectric scheme in 1967, which led to the  
271 derivation of a part of the discharge. Consequently, a new gauging station was installed 2 km downstream

272 from the original one, downstream from the restitution of the derived discharges. This station, logically  
 273 named "Beaucaire Restitution" (Kilometric point 269.5), has been used ever since. This resulted in a data  
 274 gap during the construction process between 1967 and 1970.

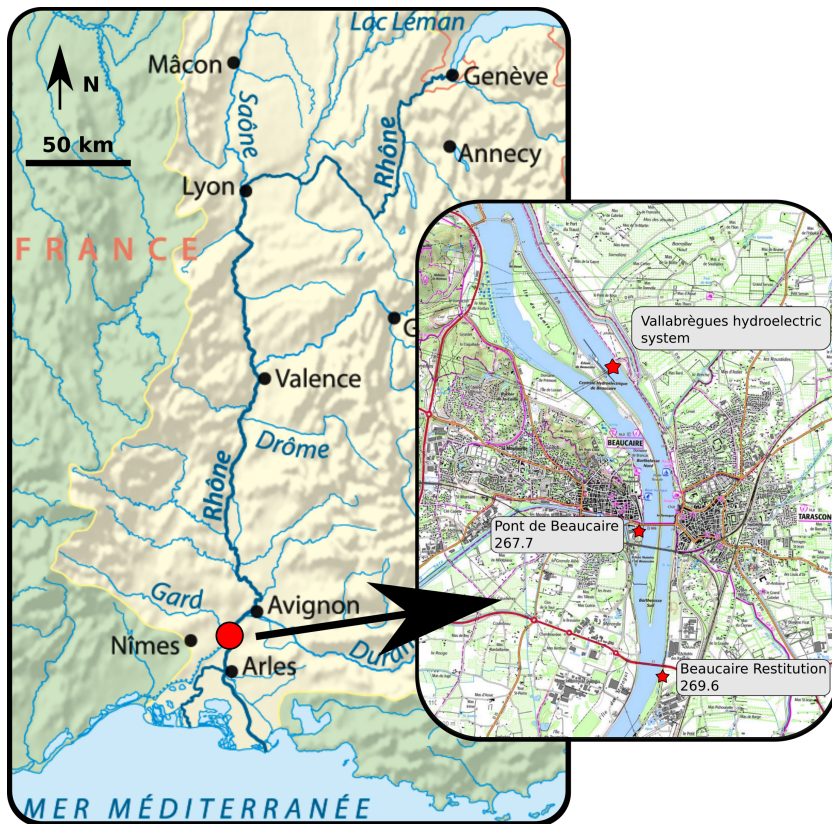


Figure 2: The French Rhône River catchment and Beaucaire gauging stations (from [www.geoportail.gouv.fr](http://www.geoportail.gouv.fr) and [www.openstreetmap.org](http://www.openstreetmap.org))

### 275 3.2 Rating curves

276 Many gauges of the Rhône River are subject to the effect of variable backwaters caused by the proximity of  
 277 a dam, and therefore require the use of a stage-fall-discharge (SFD) rating curve model (for example, Valence  
 278 gauge, 140 km upstream from Beaucaire described by Mansanarez, 2016). Beaucaire is located within a  
 279 narrowing of the floodplain and there is no dam downstream from the gauge. However, a backwater effect  
 280 from the sea has been observed at Beaucaire Restitution, but it only affects the very low flows. As this  
 281 article focuses on floods, we assume that there is no reason to use a SFD model here. Consequently, like  
 282 the gauge operator (CNR), a stage-discharge (SD) model is used for both Pont de Beaucaire and Beaucaire  
 283 Restitution gauges.

#### 284 3.2.1 Pont de Beaucaire

285 At Pont de Beaucaire, the stage-discharge relationship can be approximated by two additive channel controls:  
 286 a main channel and a floodway. Thus, the rating curve equation can be written as follows:

$$Q(h) = \begin{cases} a_1(h - b_1)^{c_1}, & \text{if } \kappa_1 < h \leq \kappa_2 \text{ (main channel)} \\ a_1(h - b_1)^{c_1} + a_2(h - b_2)^{c_2}, & \text{if } h > \kappa_2 \text{ (main channel + floodway)} \end{cases} \quad (2)$$

287 Within the main channel (when water stage is below  $\kappa_2 \approx 2$  m), the flow is splitted in two sub-channels  
 288 (figure 3b) since time immemorial (at least before 1816) as described by Armand (1907). The mobile sandbars  
 289 separating the flow were progressively fixed by dikes during the XIX<sup>th</sup> Century to ease the navigation (figure  
 290 3a). These sub-channels are connected upstream and downstream from the gauge location, thus they can be  
 291 modelled as a single main channel whose average width ( $\approx 300$  m) is the sum of the two sub-channels widths  
 292 (figure 3b). When stage exceeds  $\kappa_2$ , water starts flowing on the sandbars between the two subchannels. At  
 293 the gauge location, the total width is limited by unsubmersible levees, but a floodway is also activated a  
 294 few hundred meters downstream from the station, impacting the stage-discharge relationship at the gauge.  
 295 The width of this floodway is around 500 m.

296 The prior distributions of the rating curve parameters are specified using historical material retrieved  
 297 in regional archives, as described in table 1. Physical parameters that have a direct hydraulic meaning  
 298 are expressed in the first three lines: channel width ( $B$ ), slope ( $S$ ) and Strickler coefficient ( $K$ ). The  
 299 resulting prior distribution for the inferred parameter  $a = KB\sqrt{S}$  is deduced by Monte Carlo propagation.  
 300 Log-normal priors are used for positive quantities such as slopes, channel widths and Strickler coefficients.  
 301 Informative but imprecise priors are assigned to parameters such as channel widths, slopes or offsets which  
 302 can be difficult to estimate precisely. For  $c$  exponents, very precise priors are used because they depend  
 303 on the control type and shape (here  $c = 5/3$  for wide rectangular channel controls based on the simplified  
 304 Manning-Strickler equation as described by Le Coz et al. (2014b)). Structural uncertainty parameters have  
 305 uninformative priors.

306 According to historical profiles and cross-sections, we assume that changes affecting main channel and  
 307 floodway controls may have occurred due to major floods (in particular 1840, 1856 and 1935 floods) and  
 308 that channel widths remained constant. Those changes are called "overall changes" and are supposed to  
 309 affect both main channel and floodway offsets ( $b_1$  and  $b_2$ ) at the same time. Meanwhile, we assume that  
 310 local changes due to dike works or sediment depositions from small floods affected the offset ( $b_1$ ) of the main  
 311 channel only. As described by Mansanarez et al. (2019a), local and overall changes  $\Delta_l^{(k)}$  and  $\Delta_g^{(k)}$  affect the  
 312 offsets of two consecutive periods (( $k - 1$ ) and  $k$ ) as follows:

$$\begin{cases} b_1^{(k)} = b_1^{(k-1)} - (\Delta_g^{(k)} + \Delta_l^{(k)}), & \text{(incremental changes in the main channel)} \\ b_2^{(k)} = b_2^{(k-1)} - \Delta_g^{(k)}, & \text{(incremental changes in the floodway)} \end{cases} \quad (3)$$

313 As the most recent period obtained by gaugings segmentation is assumed to be the most accurately  
 314 known, it is used as the reference period ( $k = 1$ ) and periods are numbered backward in time. Prior  
 315 distributions of offset changes are determined in section 3.2.3.

316 **3.2.2 Beaucaire Restitution**

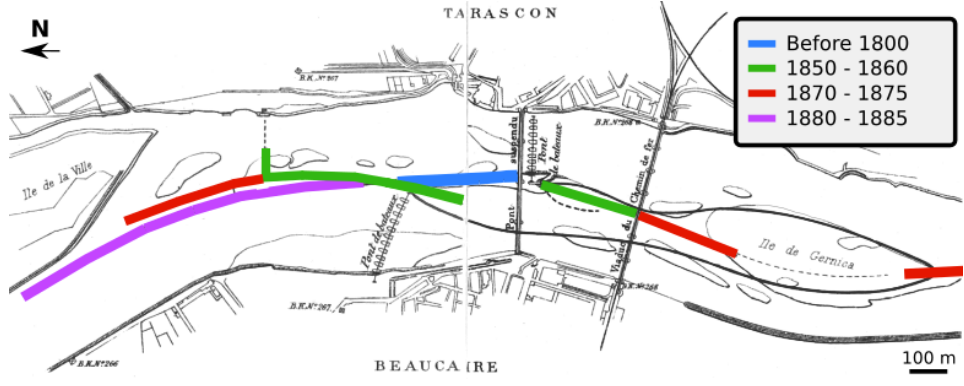
317 Beaucaire Restitution station has a quite stable profile according to 1974-2016 cross-sections (figure 3c left),  
 318 but the stage-discharge relationship is known to be influenced by the Mediterranean Sea level variations for  
 319 very low flows (this influence does not apply to the Pont de Beaucaire gauge, located 2 kilometers upstream).  
 320 This backwater effect can be represented by a channel control with a slope smaller than the slope of the  
 321 uniform flow, i.e. the mean slope of the channel. The first control (representing low flows influenced by the  
 322 sea) therefore has the same geometry as the second control (the main channel), but a smaller slope. The  
 323 main channel control is not influenced by the sea and its slope is close to the longitudinal river slope.

324 At the gauge location, the 12 meters high banks prevent overbank flows (figure 3c left). However, overbank  
 325 flows occur further downstream on the left bank, for stages higher than approximately 8 m (figure 3c right).  
 326 A floodway control (additive to the main channel) is activated above  $\approx 8$  m to model those overbank flows.  
 327 Therefore, the rating curve equation can be written as follows:

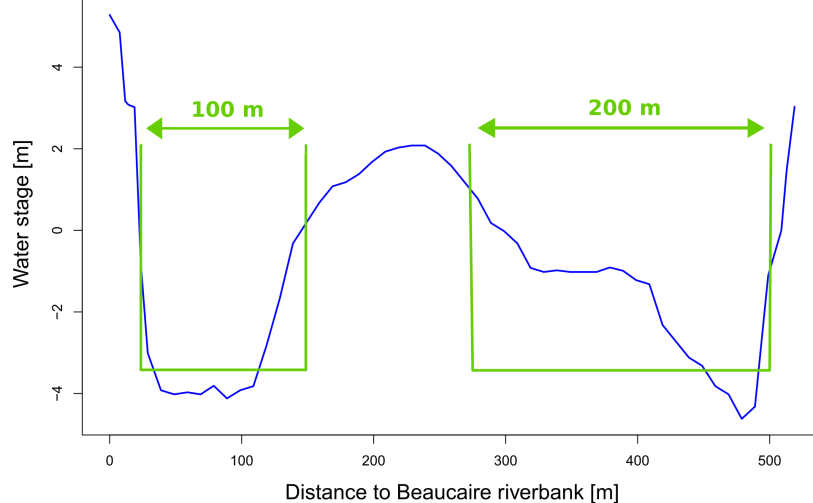
$$Q(h) = \begin{cases} a_1(h - b_1)^{c_1}, & \text{if } \kappa_1 < h \leq \kappa_2 \text{ (main channel, sea-influenced)} \\ a_2(h - b_2)^{c_2}, & \text{if } \kappa_2 < h \leq \kappa_3 \text{ (main channel, non-influenced)} \\ a_2(h - b_2)^{c_2} + a_3(h - b_3)^{c_3} & \text{if } h > \kappa_3 \text{ (main channel + floodway)} \end{cases} \quad (4)$$

328 Prior distributions of rating curve parameters are specified using recent maps and cross-sections. Priors  
 329 of the influenced and non-influenced main channels offsets  $b_1$  and  $b_2$  are assumed Gaussian with mean the  
 330 riverbed elevation that is approximately equal to -5 m. Those offsets  $b_1$  and  $b_2$  are assumed changing in  
 331 parallel (same local changes as the controls are in the same channel) due to a bed erosion trend described in  
 332 section 3.2.3, whereas floodway offset  $b_3$  and channel widths are supposed constant because of fixed dikes.  
 333 These "local changes"  $\Delta_l^{(k)}$  are computed backwards in time as follows:

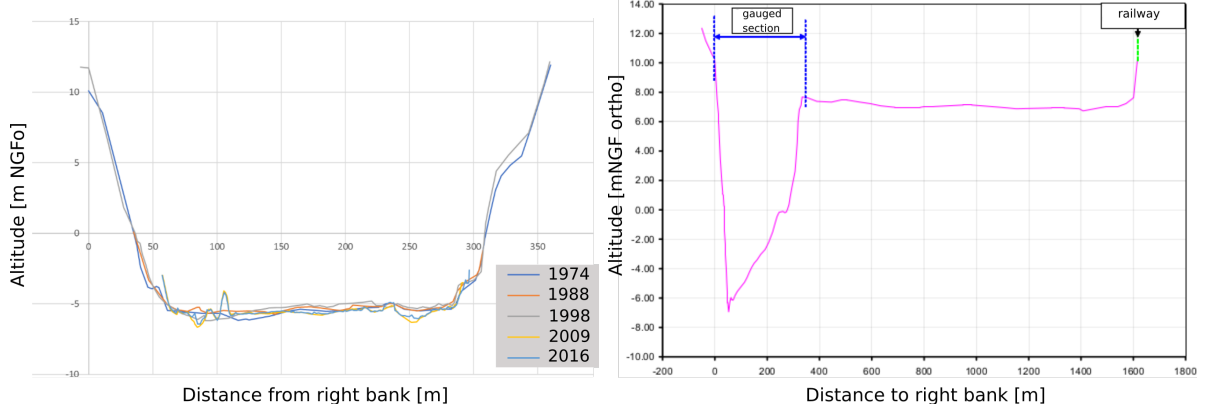
$$\begin{cases} b_1^{(k)} = b_1^{(k-1)} - \Delta_l^{(k)}, & \text{(incremental changes in the main channel)} \\ b_2^{(k)} = b_2^{(k-1)} - \Delta_l^{(k)}, & \text{(incremental changes in the floodway)} \end{cases} \quad (5)$$



(a)



(b)



(c)

Figure 3: Historical geometry of the Rhône river near Beaucaire: (a) Map of dike evolution between 18<sup>th</sup> and 20<sup>th</sup> centuries, adapted from Armand (1907); (b) Approximation of the two subchannels composing the main channel control, based on a 1845 cross-section survey; (c) Profiles from 1974 to 2016 (left) at Beaucaire Restitution station and 2.5 km downstream from the station (right) from CNR data, translated from Bard and Lang (2018) and MEDD (2005)

335 **3.2.3 Prior estimation of bed changes**

336 It is possible to follow the evolution of riverbed elevation through the evolution of yearly lowest stages. Here,  
 337 the 5% annual stage quantile is considered (figure 4). At Pont de Beaucaire (1816 - 1967), the 5% quantile  
 338 is oscillating with a 0.3 m standard deviation. Those variations do not seem to be related to the occurrence  
 339 of major floods. Without more precise information, we assume that prior distributions of local and overall  
 340 offset changes defined in section 3.2 are Gaussian with mean zero and standard deviation 0.3 (table 1).

341 At Beaucaire Restitution (1970-2020), the annual 5% quantile shows a large decrease during the first 4  
 342 years (more than 1 m). This is a consequence of Vallabregues hydraulic works between 1967 and 1970 as  
 343 well as substantial dredgings. A geomorphic adjustment after the works in the channel may have affected  
 344 the riverbed level as well. After the first years, the channel bottom stabilized, however with a slight scouring  
 345 trend of about 30 cm in 40 years. The standard deviation of the 5% quantiles reaches 0.5 m. Those bed  
 346 elevation changes affect both sea-influenced and non-influenced main channel controls offsets. Therefore,  
 347 the prior distribution of local changes is assumed Gaussian, with mean zero and standard deviation 0.8 m,  
 348 which is larger than 0.5 m to be more representative of the large changes that occurred during the first years  
 349 (table 2).

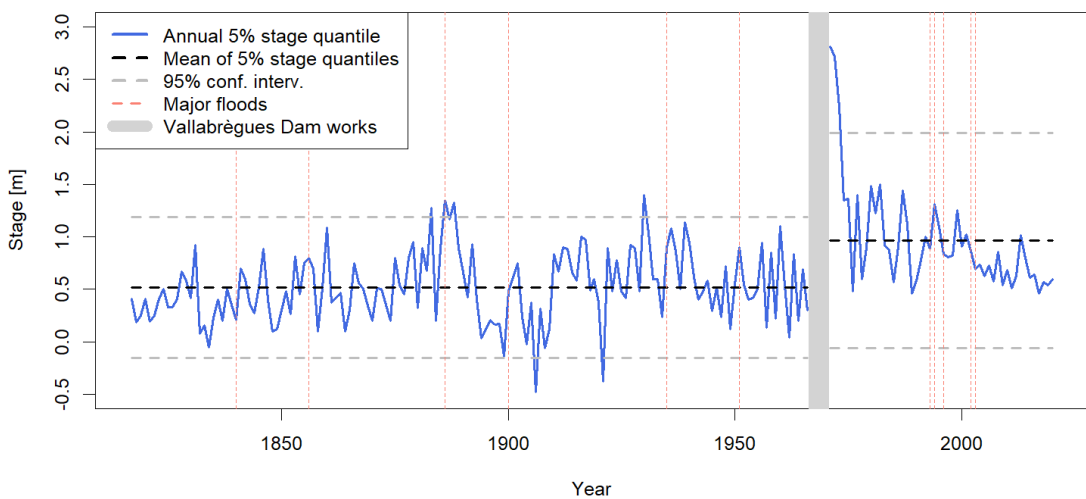


Figure 4: Time series of annual 5% stage quantile at both Pont de Beaucaire (1816-1967) and Beaucaire Restitution (1970-2020) stations.

Physical param.	Meaning	Prior	Inferred param.	Prior
<b>Control 1: main channel</b>				
$b_1[m]$	Offset	$\mathcal{N}(-4, 0.5)$	$b_1[m]$	$\mathcal{N}(-4, 0.5)$
$B_1[m]$	Channel width	$\mathcal{LN}(\ln(300), 0.16)$	$a_1[m^{3/2}/s]$	$\mathcal{LN}(\ln(128.6), 1.8 \cdot 10^{-2})$
$K_1[m^{1/3}/s]$	Strickler coeff.	$\mathcal{LN}(\ln(35), 0.14)$		
$S_1[m/m]$	Bed slope	$\mathcal{LN}(\ln(1.5 \cdot 10^{-4}), 0.55)$		
$c_1[-]$	Exponent	$\mathcal{N}(5/3, 0.025)$	$c_1[-]$	$\mathcal{N}(5/3, 0.025)$
<b>Control 2: floodway</b>				
$b_2[m]$	Offset	$\mathcal{N}(1.5, 0.5)$	$b_2[m]$	$\mathcal{N}(2, 0.5)$
$B_2[m]$	Channel width	$\mathcal{LN}(\ln(500), 0.1)$	$a_2[m^{3/2}/s]$	$\mathcal{LN}(\ln(241.9), 1.10^{-2})$
$K_2[m^{1/3}/s]$	Strickler coeff.	$\mathcal{LN}(\ln(30), 0.16)$		
$S_2[m/m]$	Bed slope	$\mathcal{LN}(\ln(2.6 \cdot 10^{-4}), 0.34)$		
$c_2[-]$	Exponent	$\mathcal{N}(5/3, 0.025)$	$c_2[-]$	$\mathcal{N}(5/3, 0.025)$
<b>Structural uncertainty parameters</b>				
$\gamma_1[m^3/s]$	Intercept	$\mathcal{U}(0, 1000)$	$\gamma_1[m^3/s]$	$\mathcal{U}(0, 1000)$
$\gamma_2[-]$	Slope	$\mathcal{U}(0, 100)$	$\gamma_2[-]$	$\mathcal{U}(0, 100)$
<b>Multiperiod RC parameters</b>				
$\Delta l[m]$	Local change	$\mathcal{N}(0, 0.3)$	$\Delta l[m]$	$\mathcal{N}(0, 0.3)$
$\Delta g[m]$	overall change	$\mathcal{N}(0, 0.3)$	$\Delta g[m]$	$\mathcal{N}(0, 0.3)$

Table 1: Priors elicitation for Pont de Beaucaire rating curves.  $\mathcal{U}(a, b)$  stands for continuous uniform distribution with bounds  $a$  and  $b$ ,  $\mathcal{N}(\mu, \sigma)$  for Normal distribution with mean  $\mu$  and standard deviation  $\sigma$ , and  $\mathcal{LN}(\mu, \sigma)$  for Log Normal distribution with mean  $\mu$  and standard deviation  $\sigma$ .

Physical param.	Meaning	Prior	Inferred param.	Prior
<b>Control 1: Low flows sea-influenced channel</b>				
$b_1[m]$	Offset	$\mathcal{N}(-5, 0.5)$	$b_1[m]$	$\mathcal{N}(-5, 0.5)$
$B_1[m]$	Channel width	$\mathcal{LN}(\ln(300), 0.32)$	$a_1[m^{3/2}/s]$	$\mathcal{LN}(\ln(49.50), 3.2 \cdot 10^{-2})$
$K_1[m^{1/3}/s]$	Strickler coeff.	$\mathcal{LN}(\ln(35), 0.14)$		
$S_1[m/m]$	Bed slope	$\mathcal{LN}(\ln(5.10^{-5}), 0.20)$		
$c_1[-]$	Exponent	$\mathcal{N}(5/3, 0.025)$	$c_1[-]$	$\mathcal{N}(5/3, 0.025)$
<b>Control 2: Main channel</b>				
$b_1[m]$	Offset	$\mathcal{N}(-5, 0.5)$	$b_1[m]$	$\mathcal{N}(0, 0.5)$
$B_1[m]$	Channel width	$\mathcal{LN}(\ln(300), 0.32)$	$a_2[m^{3/2}/s]$	$\mathcal{LN}(\ln(148.49), 2.4 \cdot 10^{-2})$
$K_1[m^{1/3}/s]$	Strickler coeff.	$\mathcal{LN}(\ln(35), 0.14)$		
$S_1[m/m]$	Bed slope	$\mathcal{LN}(\ln(2.10^{-4}), 0.25)$		
$c_1[-]$	Exponent	$\mathcal{N}(5/3, 0.025)$	$c_2[-]$	$\mathcal{N}(5/3, 0.025)$
<b>Control 3: Floodway</b>				
$b_3[m]$	Offset	$\mathcal{N}(8, 0.5)$	$b_3[m]$	$\mathcal{N}(8, 0.5)$
$B_3[m]$	Channel width	$\mathcal{LN}(\ln(200), 0.47)$	$a_3[m^{3/2}/s]$	$\mathcal{LN}(\ln(241.9), 1.10^{-2})$
$K_3[m^{1/3}/s]$	Strickler coeff.	$\mathcal{LN}(\ln(25), 0.20)$		
$S_3[m/m]$	Bed slope	$\mathcal{LN}(\ln(2.4 \cdot 10^{-4}), 0.21)$		
$c_3[-]$	Exponent	$\mathcal{N}(5/3, 0.025)$	$c_3[-]$	$\mathcal{N}(5/3, 0.025)$
<b>Structural uncertainty parameters</b>				
$\gamma_1[m^3/s]$	Intercept	$\mathcal{U}(0, 1000)$	$\gamma_1[m^3/s]$	$\mathcal{U}(0, 1000)$
$\gamma_2[-]$	Slope	$\mathcal{U}(0, 100)$	$\gamma_2[-]$	$\mathcal{U}(0, 100)$
<b>Multiperiod RC parameters</b>				
$\Delta l[m]$	Local change	$\mathcal{N}(0, 0.8)$	$\Delta l[m]$	$\mathcal{N}(0, 0.8)$

Table 2: Priors elicitation for Beaucaire Restitution rating curves.  $\mathcal{U}(a, b)$  stands for continuous uniform distribution with bounds  $a$  and  $b$ ,  $\mathcal{N}(\mu, \sigma)$  for Normal distribution with mean  $\mu$  and standard deviation  $\sigma$ , and  $\mathcal{LN}(\mu, \sigma)$  for Log Normal distribution with mean  $\mu$  and standard deviation  $\sigma$ .

350 **3.3 Stage series**

351 **3.3.1 Pont de Beaucaire (1816 - 1967)**

352 Thanks to the archival work of Pichard et al. (2017), a continuous stage series at Pont de Beaucaire from  
 353 1816 to 1967 is available with daily stage readings from 1816 to 1840, and three stage readings per day from  
 354 1841 to 1967. The records were made visually by an operator, at noon during the first years, then at 7am,  
 355 12am and 5pm (Figure 5). When three stage readings per day are available, the maximum of the three  
 356 stages is considered as the daily maximum stage, and before 1840 the unique value at noon is kept as the  
 357 daily maximum stage. Additionally, after 1840, when the stage was rising above 5 m, the operators made  
 358 more frequent visual records (supposedly hourly measurements). When these records are available, they are  
 359 of course used to establish the daily maximum stages.

DATES	OBSERVATIONS ORDINAIRES			ÉTAT DU CIEL	VENT	RENNSEIGNEMENTS DIVERS.
	7 h.	midz.	5 h.			
	m.	in.	m.			(On mettra sur l'astuce par les observations des crues.)
1	2.56	2.54	2.54	peu nuageux	vent fort	
2	2.50	2.44	2.38	nuageux	vent Est	faible
3	2.24	2.16	2.14	peu d.	vent Ouest	assez fort
4	2.04	2.00	1.98	des d.	vent	faible
5	1.89	1.84	1.80	nuageux	vent	vent
6	1.76	1.72	1.72	des gouttes	calme	
7	1.75	1.80	1.92	nuageux	vent Ouest	modérée
8	2.62	3.02	3.36	peu d.	vent Est	faible
9	3.82	3.90	3.98	averse d.	vent Est	T
10	4.10	4.16	4.25	des averses	vent Est	assez fort T

Figure 5: Table of limnimetric surveys at Pont de Beaucaire, March 1914. Operators were supposed to provide the water level at 7am, 12am and 5pm, as well as a few meteorologic details. (Ponts\&Chaussées, 1914)

360 Stage uncertainties depend on the measurement method, as described in section 2.3. Table 3 summarizes  
 361 the different sources of stage uncertainties at Beaucaire, here given as standard deviations  $\sigma$ . Staff gauge  
 362 reading uncertainty  $\sigma_1$  is taken as 5 cm. Staff gauge precision is centimetric, but as this work is focused on  
 363 floods, the error is expanded because of the waves that may complicate the reading. Sensor precision  $\sigma_2$  and  
 364 sensor calibration uncertainties  $\sigma_3$  are not considered at Pont de Beaucaire as the stage was read by operators  
 365 directly on the staff gauge. Bard and Lang (2018) have compiled several elevation measurements of the staff  
 366 gauge datum between 1912 and 2010. Most of those measurements occurred after the decommissioning  
 367 of Pont de Beaucaire station. Datum uncertainty  $\sigma_4$  is assumed to be equal to the standard deviation of  
 368 those measurements: 6 cm. The datum measurement frequency during the operation of Pont de Beaucaire  
 369 station is assumed to be 25 years (i.e. the average duration between the retrieved elevation measurements).  
 370 Hence, datum errors are drawn every 25 years. As described in section 2.3, the distribution of measurement

frequency errors  $\delta_5$  can be estimated using the frequent stage measurements at Beaucaire Restitution between 1970 and 2020 (50 AMAX values). For the "one stage reading per day" case (mimicking the 1816-1840 period), this error corresponds to the difference between the maximum hourly stage value and the stage at noon of the same day. The "three stage readings per day" error (1840-1967) is the difference between the maximum hourly stage of a day, and the maximum of 7am, noon and 5pm stages of the same day. An exponential distribution is estimated for both errors samples and is used to represent the measurement frequency uncertainty affecting the annual maximum stages at Pont de Beaucaire. According to gauge management instructions, hourly measurements were made by observers after 1840, and for the stages above 5 meters. Hence, measurement frequency error  $\delta_5$  can be considered as negligible when stage is above 5 meters after 1840.

SYMADREM (2012), Pichard (2013) and Bard and Lang (2018) suggested that for the floods during which dike breaks happened downstream from Beaucaire, stage measurements should be corrected because the stage measured at the station may lead to underestimating the actual discharge of the flood. The stage corrections for the more thoroughly studied floods of 1840, 1841 and 1856 estimated by SYMADREM (2012) are adopted. For these floods stage uncertainty is represented by a Gaussian distribution, with mean the estimated stage and standard deviation half of the applied correction, chronologically: 0.94, 0.4 and 0.4 m.

### 3.3.2 Beaucaire Restitution (1970 - 2020)

For Beaucaire Restitution station, most of the stage uncertainty values come from CETIAT (2005) expertise on behalf of Compagnie Nationale du Rhône. They are summarized in table 3. Staff gauge reading uncertainty is considered zero as the measurements are done by automatic sensors. Instrument precision uncertainty:  $\sigma_2 = 0.01/\sqrt{3}$  m comes from the sensor manufacturer specifications. The standard deviation of all the re-calibrations made by the operators is equal to 5 cm according to CETIAT (2005). Calibration is also affected by staff gauge reading uncertainties, because the stage read on the staff gauge is the reference used by operators to calibrate the sensor. CETIAT (2005) estimated a 3.35 cm uncertainty for the gauge reading uncertainty. Therefore, gauge reading and calibration uncertainties are combined as follows:  $\sigma_3 = \sqrt{0.0335^2 + 0.05^2} = 0.06$  m. As the average time lag between calibrations is 6 months, a new value of the error  $\delta_3$  is drawn for each annual maximum stage. Datum reference uncertainty  $\sigma_4$  is considered negligible because of the precision of modern topographic measurements (< 1 cm). Measurement frequency uncertainty  $\sigma_5$  is considered negligible, because the sub-hourly measurement frequency is assumed adequate to capture the Rhône River stage variability.

Date	$\delta_1$ : gauge reading	$\delta_2$ : sensor precision	$\delta_3$ : sensor calibration	$\delta_4$ : datum reference	$\delta_5$ : measurement frequency	
					Stage < 5m	Stage $\geq$ 5m
Before 1840	$\mathcal{N}(0, 0.05)$	-	-	$\mathcal{N}(0, 0.06)$	$Exp(2.18)$	
1840 - 1967	$\mathcal{N}(0, 0.05)$	-	-	$\mathcal{N}(0, 0.06)$	$Exp(8.86)$	-
1970 - 2020	-	$\mathcal{N}(0, 0.01/\sqrt{3})$	$\mathcal{N}(0, 0.06)$	-	-	-

Table 3: Distributions used for the different sources of stage errors (in meters).  $\mathcal{N}$ (mean, st. deviation) and  $Exp$ (rate) represent Gaussian and Exponential distributions. As a reminder, the periods before 1967 are associated with the Pont de Beaucaire station and the period 1970-2020 with the Beaucaire Restitution station

#### 401 3.4 Gaugings **discharge measurements**

402 A set of 244 gaugings from 1840 to 1967 has been compiled at Pont de Beaucaire. After excluding  
 403 a few gaugings which were considered dubious, 233 measurements remain. The frequency of gaugings is  
 404 variable in time. No gaugings were retrieved before 1840 and there are several 10- to 20-year gaps without  
 405 gaugings, which makes the estimation of the stage-discharge relationship over time challenging. The assumed  
 406 uncertainty of the gaugings at Beaucaire depends on the gauging method according to Bard and Lang (2018)  
 407 values specified in table 4.

408 A set of 304 gaugings is available at Beaucaire Restitution. A few of these were out of the period of stage  
 409 measurements availability and were discarded. Finally, 296 gaugings were selected. As modern hydrometric  
 410 developments allowed estimating the uncertainty for each individual gauging (particularly for ADCP and  
 411 current meters), those values are used when available in the CNR archives. If not, values from table 4 are  
 412 considered.

Gauging method	Standard uncertainty
Current meter at 0.6 h and surface	5%
Current meter point by point	3.5%
Surface current meter	7.5%
Unknown type	7.5%
ADCP	3.5%
Floats before 1936	10%
Hydrotachymeter before 1936	10%

Table 4: Gaugings uncertainty depending on the method used (hypotheses from Bard and Lang (2018)). Expressed as standard deviations of the measured discharge in %.

413 **4 Results**

414 **4.1 Assessment of rating shifts**

415 Darienzo et al. (2021) segmentation procedure is applied at Beaucaire as described in section 2.1. The prior  
 416 for the residual mean during each sub-period is taken as a Gaussian distribution with zero mean and a 500  
 417  $\text{m}^3/\text{s}$  standard deviation for both stations. The maximum number of segments at each iteration is fixed at  
 418 six (see Darienzo et al. (2021) for details on priors and parameters specification).

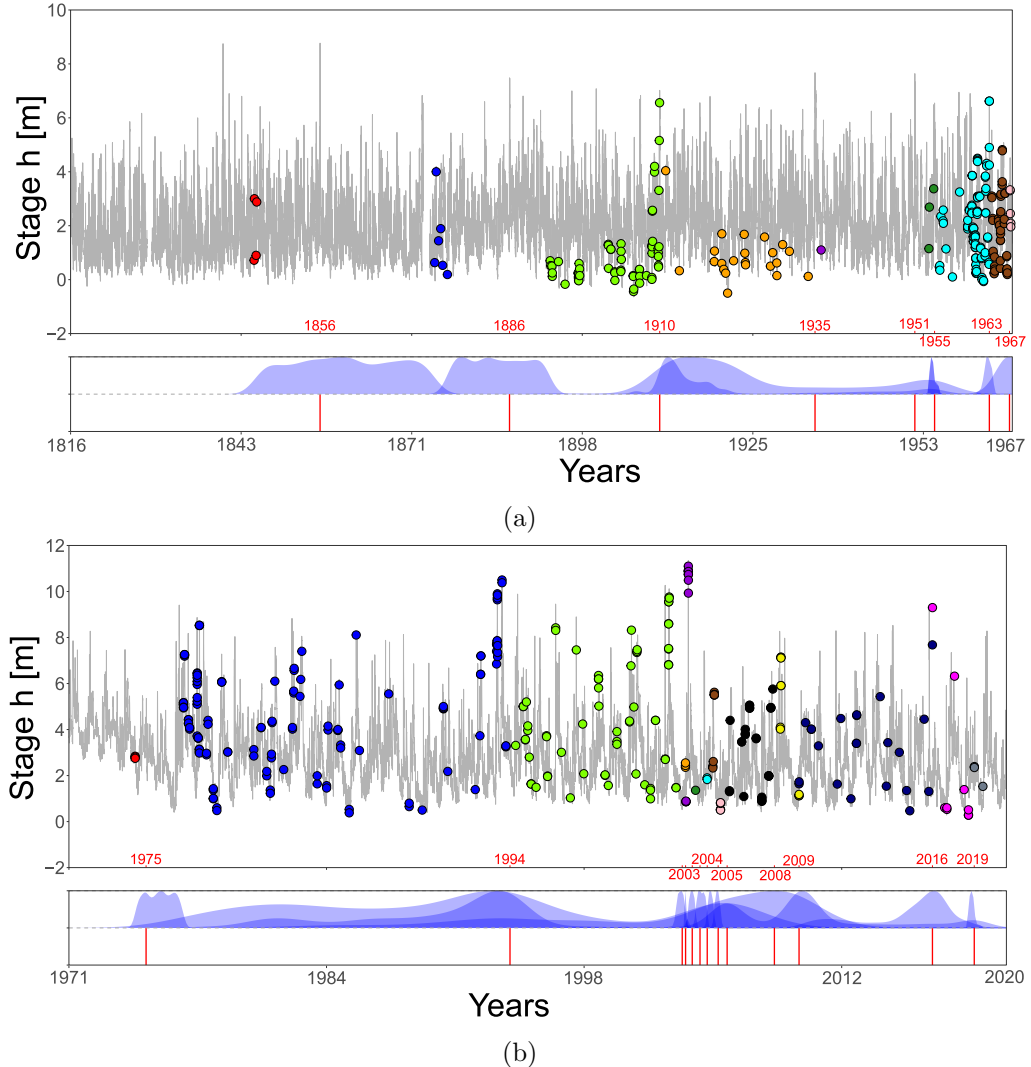


Figure 6: Gaugings segmentation of the Rhône River at Pont de Beaucaire (a) and Beaucaire Restitution (b). Dots represent gaugings with different colors for each stable period. The grey curve is the stage series. Blue ribbons represent posterior pdf of shift times and red segments are the retained shift times taken as the maximum stage included in each posterior pdf interval.

419 Eight shift times are detected at Pont de Beaucaire (Figure 6 left). The gauging frequency is not constant  
 420 through the history of the station and some periods include a small number of gaugings. As a consequence,  
 421 the posterior pdfs of shift times span over many years for the first shifts, and are similar to uniform distri-  
 422 butions between sets of gaugings. This is reassuring about the method since there is indeed no information

423 during long no-gauging periods to identify a shift time. Without discharge measurement (gaugings) the  
424 method is not able to detect any rating shifts. Additional information may be of interest for those first  
425 periods. It is no surprise that most of the shifts occur very close to the largest historical floods. 1935 and  
426 1951 shifts respectively correspond to the 3<sup>rd</sup> and 4<sup>th</sup> largest floods of the history of the station. There is, by  
427 construction of the segmentation model, no shift before 1845, year of the first available gaugings. However,  
428 we can consider that the 1840 flood (supposedly the largest flood since 1800) is likely to have caused a shift.  
429 Therefore, an additional shift time is added at the exact flood date. This brings the total number of stable  
430 periods to 10 (table 5).

431 Thirteen shift times are detected at Beaucaire Restitution. As can be seen in figure 6 (right), gauging  
432 frequency is far higher than for Pont de Beaucaire station (except during the first 5 years), resulting in a  
433 better determination of the rating shift times. Due to the lack of gaugings at the beginning of the series, only  
434 one rating shift is detected but many shifts potentially took place in those first four years as morphological  
435 adjustment and dredging occurred (see section 3.2.3). This first shift is assumed to be assigned to the first  
436 large flood of the station in 1976, after which the channel stabilized. The next shift occurred during the  
437 1994 flood, one of the largest at the station. The most notable flood at Beaucaire Restitution occurred in  
438 2003 (11 500 m<sup>3</sup>/s, with a return period of about 100 years according to MEDD (2005)). Unsurprisingly,  
439 the stage-discharge relationship is considerably disrupted by this event, as reflected by the six rating shifts  
440 detected from 2003 to 2005. Two out of these six shifts were discarded because the shift amplitude is  
441 considered minor based on further analysis of the corresponding rating curve change. The largest flood  
442 within posterior intervals of those shifts almost always corresponds to the 2003 flood. This is also the case  
443 for 2005, 2008 and 2009 shifts, for which the posterior pdf spans many years including 2003. Therefore, the  
444 shift dates are assumed to be located to the maxpost shift times, as several shifts cannot be located at the  
445 same date. The last shift of 2019 is also discarded because the shift amplitude is considered minor based on  
446 further analysis. Finally, ten rating shifts are retained. This brings the number of stable periods to eleven  
447 for Beaucaire Restitution (table 5).

448

Maxpost shift time	Largest flood within <i>post. pdf</i>	Final choice	Period number	Number of gaugings
<b>Pont de Beaucaire (1816-1967)</b>				
No gaugings	No gaugings	1840-11-02	1	0
1860-02-20	1856-06-01	1856-06-01	2	4
1887-05-11	1886-10-29	1886-10-29	3	6
1910-11-21	1910-12-09	1910-12-09	4	58
1921-06-22	1935-11-14	1935-11-14	6	22
1954-08-08	1951-11-23	1951-11-23	6	1
1954-03-30	1955-01-23	1955-01-23	7	3
1963-03-23	1963-11-08	1963-11-08	8	91
1967-01-31	1967-01-31	1967-01-31	9	43
1967-12-31	End of stage series	End of stage series	10	5
<b>Beaucaire restitution (1970-2020)</b>				
1975-02-06	1976-11-11	1976-11-11	1	3
1994-06-10	1994-01-08	1994-01-08	2	122
2003-08-05	2002-11-27	2002-11-27	3	65
2003-10-09	2003-12-04	2003-12-04	4	17
2004-02-16	2003-12-04	No shift	X	X
2004-07-15	2003-12-04	2004-07-15	5	1
2004-12-02	2004-12-02	2004-12-02	6	2
2005-07-03	2004-12-02	No shift	X	X
2005-12-24	2003-12-04	2005-12-24	7	14
2008-06-28	2003-12-04	2008-06-28	8	28
2009-10-20	2003-12-04	2009-10-20	9	7
2016-11-21	2016-11-22	2016-11-22	10	26
2019-02-11	2018-11-24	No shift	X	X
2020-01-01	End of stage series	End of stage series	11	11

Table 5: Beaucaire rating shifts dates

## 449 4.2 Multiperiod rating curves estimation

450 Uncertain rating curves are estimated using Mansanarez et al. (2019a) SPD model, for each **stable** period  
 451 detected previously. For Pont de Beaucaire, this leads to ten rating curves that show a good adequacy with  
 452 gaugings (figure 7a). The evolution of the main channel offset ( $b_1$ ) gives indications on the evolution of bed  
 453 elevation (figure 7c). Substantial changes occurred before and after the third **stable** period with successive  
 454 increase and decrease of the offset. Those changes may be related to the channel works that occurred during  
 455 the end of the XIX<sup>th</sup> Century. Afterwards, the offset is more stable and only suggests a slight increasing  
 456 trend which may be a consequence of the filling of the channel noticed in figure 4. The widest uncertainty  
 457 interval belongs to the first period (1816-1840: dark red) for which no gaugings are available (figure 7a).  
 458 The expected range of rating curve uncertainties for flood discharges (above 6 m) varies from around 20%  
 459 for the first period, to less than 10% after 1840. Static parameters are precisely estimated and are presented  
 460 in figure 7e. The  $c$  posterior distributions are as wide as priors because  $c$  priors are already very precise as  
 461 they come from simplified Manning-Strickler formula for which the exponent is exactly 5/3.

462     Eleven uncertain rating curves were computed at Beaucaire Restitution (figure 7b). The rating curve  
463     uncertainty intervals are smaller than at Pont de Beaucaire for usual stages because of a larger number  
464     of gaugings and a smaller gaugings uncertainty: around 5% of uncertainty is estimated for floods above  
465     6 m. However, low flows uncertainty is greater than at Pont de Beaucaire, because the sustained flows  
466     of the Rhône River limits the exploration of the sea-influenced hydraulic control. Low flows gaugings  
467     are unavailable. Thus, the first control offsets  $b_1$  are not precisely estimated (figure 7d), but this has no  
468     consequences on the streamflow uncertainty of AMAX floods, for which only controls 2 and 3 are active.  
469     The first period rating curve (dark red) is shifted with respect to the other curves due to the channel  
470     adjustment and dredging operations after Vallabregues works (1967-1970). The second control offsets ( $b_2$ )  
471     globally decreases over time, showing a slight scouring trend of the channel (figure 7d). Static parameters  
472     (figure 7f) appear precisely estimated, except for the 3<sup>rd</sup> control offset  $b_3$  for which the posterior distribution  
473     is as wide as the prior.

474     There are several reasons for the significant differences between the upper parts of the rating curves for  
475     Pont de Beaucaire (figure 7a) and Beaucaire Restitution (figure 7b). First, the gauge datum (the altitude  
476     of the stream gauge zero value) correspond to 3.37 m for Pont de Beaucaire and 0.06 m for Beaucaire  
477     Restitution. In addition, as the stations are 2 km apart, their cross-sections are very different. Pont  
478     de Beaucaire cross-section corresponds to a main channel splitted in two sub-channels (figure 3b), while  
479     Beaucaire Restitution cross-section corresponds to a unique channel (figure 3c). A magnified representation  
480     of the upper parts of the rating curves is available in supplementary material (figure 2).

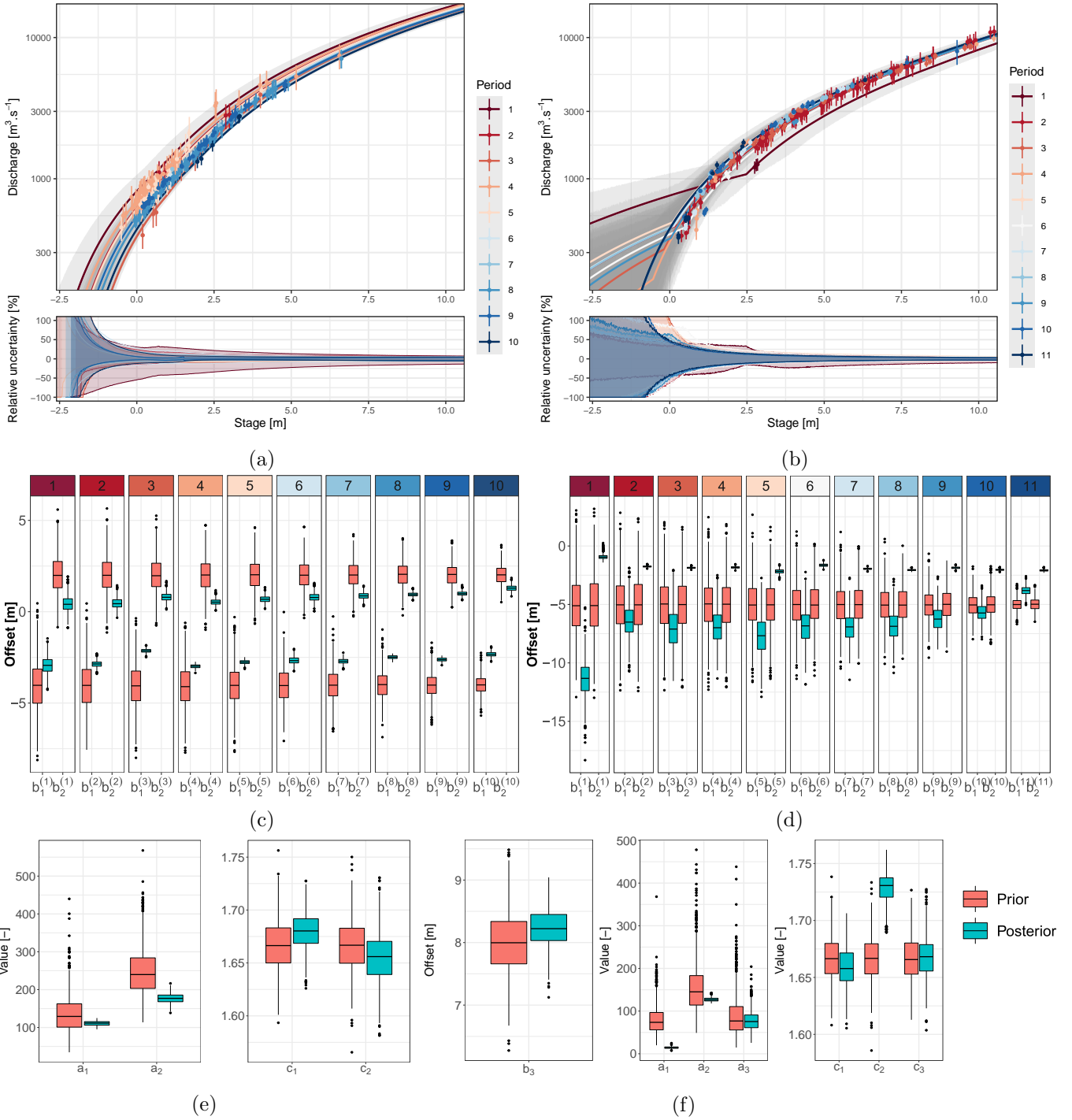


Figure 7: Pont de Beaucaire (a) and Beaucaire Restitution (b) rating curves and relative 95% uncertainty with respect to maxpost, offsets priors and posteriors (c and d) and static parameters priors and posteriors (e and f). Discharges of rating curves are in logarithmic scale, solid lines represent maxpost values, grey transparent envelopes represent 95% uncertainty intervals and dots with error bars represent the gaugings with 95% uncertainty. Stable stage-discharge periods are numbered from the oldest to the latest.

#### 481 4.3 Stage uncertainty

482 The error sources described in table 3 are combined using a Monte Carlo procedure to quantify the uncer-  
 483 tainty affecting AMAX stages as described in figure 8. The measured stage is outside and below the stage  
 484 uncertainty interval before 1840 at Pont de Beaucaire: this is due to the exponential distribution used to

485 model measurement frequency errors which are dominant during this period and are positive by definition.  
 486 The upper uncertainty bound is sometimes 1.5 meters higher than the measured stage. Therefore, con-  
 487 sidering this source of uncertainty may have substantial consequences on the final results. The difference  
 488 between uncertainty bounds and originally measured stages is presented in the bottom part of figure 8.  
 489 The uncertainty of AMAX stages decreases over time as the measurement frequency and precision improve.  
 490 The width of the 95% uncertainty interval is 1.7 m before 1840, 0.3 m between 1840 and 1967, and 0.24  
 491 m at Beaucaire Restitution (1970-2020). The 5 m threshold above which hourly measurements were done  
 492 after 1840 explains the large reduction of the uncertainty. After 1840, the uncertainty is controlled by the  
 493 exceedance of this 5 m threshold, the AMAX below 5 m being penalized by non-negligible measurement  
 494 frequency errors  $\delta_5$ .

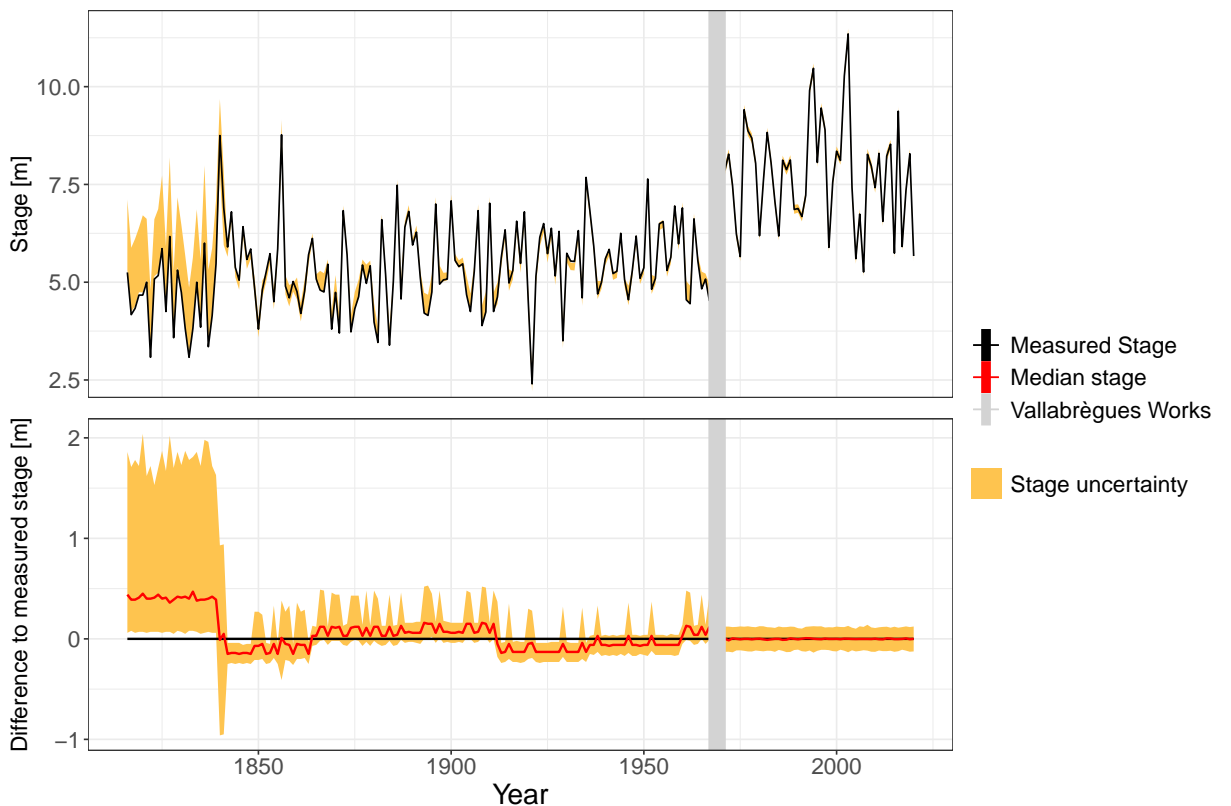


Figure 8: Top: AMAX stages and uncertainty at Beaucaire (1816-2020). Bottom: Difference between 95% stage uncertainty bounds and originally measured stage.

#### 495 4.4 Total streamflow uncertainties

496 Stage uncertainties are propagated through uncertain rating curves as described in section 2.4 and the results  
 497 are shown in figure 9. Streamflow uncertainty, although fluctuating, decreases over time from 30% before  
 498 1840, and 10% before 1967, to 5% at Beaucaire Restitution (1967-2020). This 5% uncertainty on recent  
 499 AMAX discharges is consistent with the results of the international consensus conference on the December  
 500 2003 flood : “The most likely estimate of the maximum discharge of the Rhône River at Beaucaire during

501 the December 2003 flood is 11500 m<sup>3</sup>/s, corresponding to a return period slightly above 100 years. [...]  
 502 This maximum discharge estimate is subject to an uncertainty of around 5%, resulting from the uncertainty  
 503 of flow measurements, maximum stage, parameterization and extrapolation of the December 2003 gauging  
 504 data." (MEDD, 2005).

505 Stage uncertainty appears dominant at Pont de Beaucaire, as well as rating curve parametric uncer-  
 506 tainty, originating from the difficulty to estimate rating curve parameters with only a few gaugings. Thus,  
 507 parametric uncertainty is reduced for properly gauged periods. During the Vallabregues hydraulic system  
 508 construction (1967 - 1970), the waters of the Durance River, one of the major tributaries, were deviated from  
 509 the Rhône River course. AMAX discharges of these missing years were reconstructed by CNR with upstream  
 510 gauging stations. The uncertainty around these reconstructed discharges is assumed to be represented by  
 511 a Gaussian distribution with 10% relative standard deviation. An AMAX flow (with uncertainties) time  
 512 series plot is available in supplementary material (figure 3).

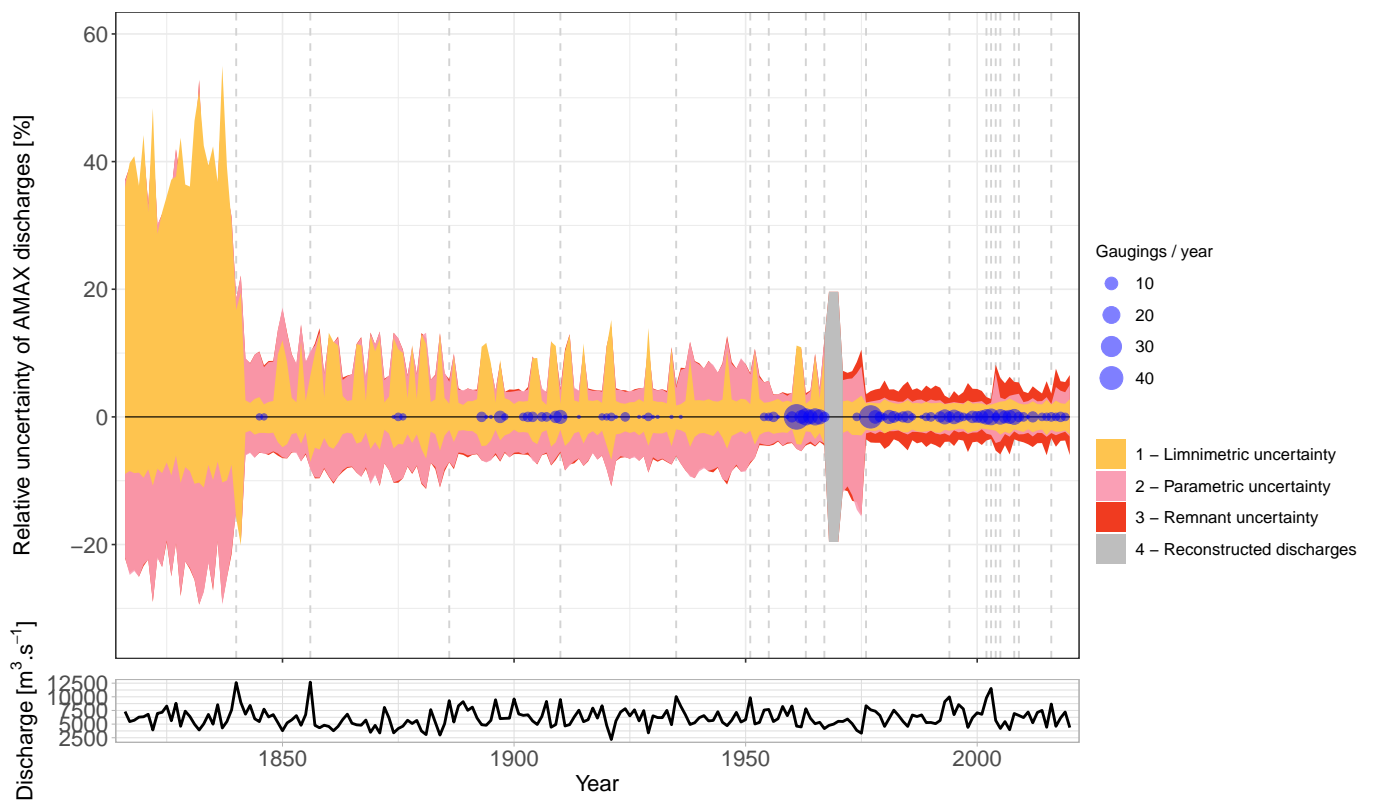


Figure 9: Relative 95% uncertainty of AMAX discharges with respect to the maxpost discharges (black solid line) for the three sources of streamflow uncertainties, at Beaucaire (1816 - 2020). Vertical dotted lines represent rating shifts.

513 **4.5 Flood frequency analysis**

514 **4.5.1 Streamflow series homogeneity**

515 The homogeneity of streamflow series is an essential prerequisite as FFA is based on the hypothesis of iid  
516 (independent and identically distributed) random variables. In order to check this hypothesis, the Mann-  
517 Kendall non-parametric test (Mann (1945); Kendall (1948)) is applied to AMAX series at Beaucaire. As  
518 streamflow uncertainty is represented by 500 AMAX discharge realizations (section 2.4), the homogeneity  
519 test is applied to each of the 500 AMAX series. Among the Mann-Kendall tests, 81% concluded to the non-  
520 rejection of the null hypothesis (there is no trend in the series) with a 0.05 significance level. We assume  
521 that this is enough to consider the series as homogeneous and to proceed to FFA.

522 **4.5.2 Flood frequency analysis**

523 The GEV distribution estimation procedure described in section 2.5 is applied to the 205-year long AMAX  
524 discharges series at Beaucaire accounting for uncertainties. Vague priors are used for GEV parameters: flat  
525 priors for location and scale parameters, and Gaussian with zero mean and 0.2 standard deviation for the  
526 shape parameter. This shape parameter prior is consistent with Martins and Stedinger (2000) suggestions.  
527 Flood quantiles results (figure 10a) show that streamflow uncertainty dominates for the lowest return periods,  
528 but sampling uncertainty becomes dominant when the return period tends toward 1000 years (see figure  
529 10c bottom right for a better understanding of the respective part of each source of uncertainty in this 205  
530 years case). The observed AMAX discharges display a large variability of streamflow uncertainties. The  
531 three largest floods of this 205 years sample (1840, 1856 and 2003, by chronological order and from the most  
532 uncertain to the most precise) illustrate this point. Thus, not considering 1840 and 1856 floods could have a  
533 strong effect on the estimation of the maxpost quantiles values, as well as their uncertainty. This is explored  
534 next by varying the sample size.

535 **4.5.3 Sample size influence on quantiles uncertainty**

536 With an exceptionally long sample at Beaucaire, the influence of sample size on flood quantiles estimation in  
537 a real case can be quantified, hence assessing the interest of using old hydrometric data when available. Four  
538 sample sizes are tested, taken as the last 50 years, 100 years, 150 years, and the largest available sample of  
539 205 years. A figure describing these sub-samples along the AMAX time series is available in supplementary  
540 material (figure 3). GEV distributions are estimated and the contribution of both streamflow and sampling  
541 uncertainties is computed for each case, following section 2.5 procedure. Total uncertainty is clearly reduced  
542 between the 50 years sample and the other samples for the three return periods: 10, 100 and 1000 years  
543 (figure 10b). Surprisingly, for the 1000-year flood estimation, the total uncertainty is not reduced between

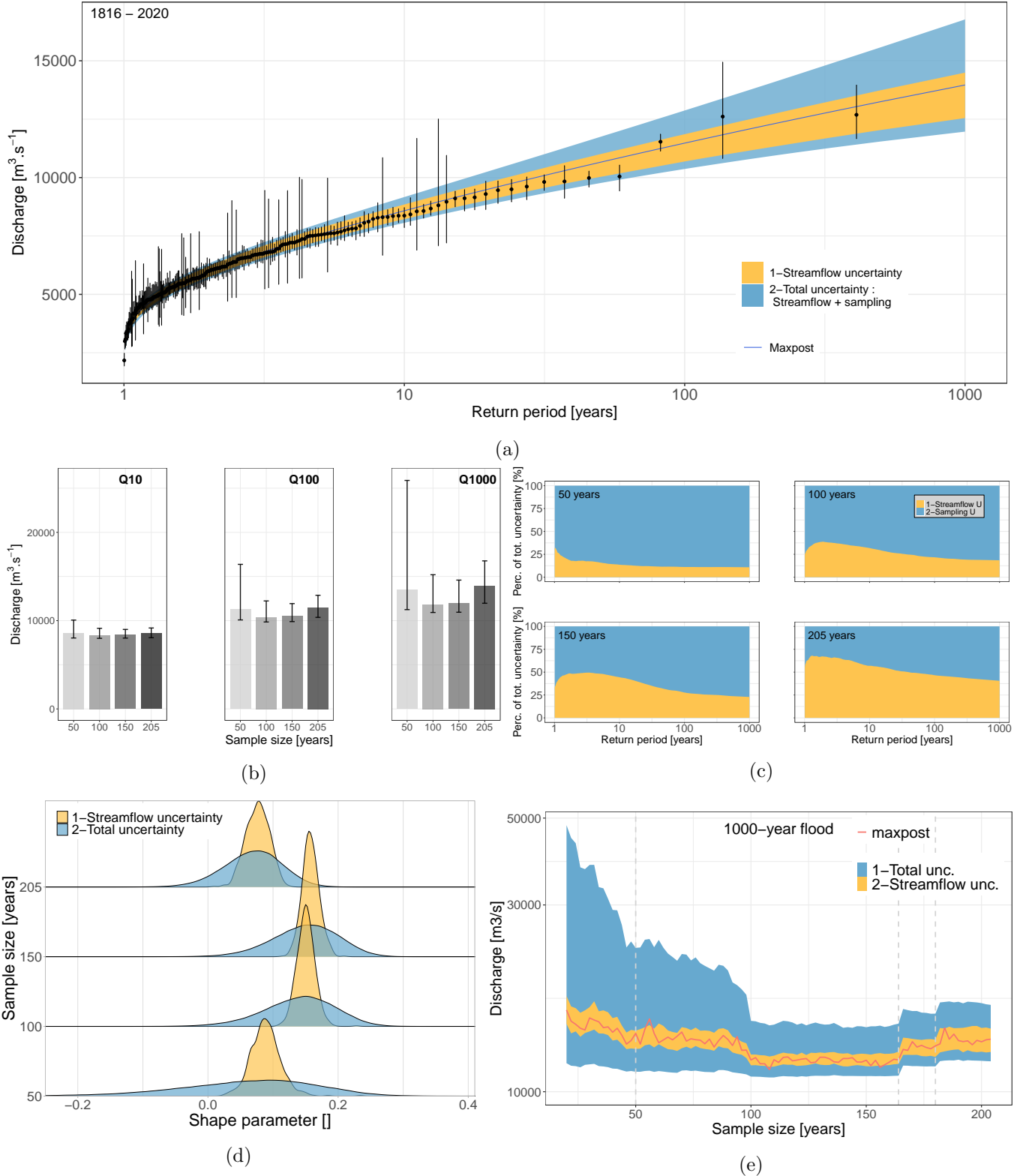


Figure 10: FFA results of the Rhône River at Beaucaire. (a) GEV distribution estimated with the full sample (1816-2020). Error bars represent the observed AMAX discharges with their 95% streamflow uncertainty. (b) Maxpost quantiles estimates for three return periods and four sample sizes. Error bars represent 95% total uncertainty intervals. (c) Contribution of streamflow and sampling uncertainties to the total uncertainty for four sample sizes. (d) GEV shape parameter distributions considering streamflow or total uncertainty for four sample sizes. (e) 1000-year flood estimations for various sample sizes. Grey dotted lines represent large changes in the sample data (the change from Pont de Beaucaire to Beaucaire Restitution gauge en 1967, the inclusion of 1856 flood and the inclusion of 1840 flood to the sample).

544 the 100 and 205 years samples. This illustrates that the reduction of sampling uncertainty induced by  
545 increasing the sample size may be compensated by the increased streamflow uncertainty when going back in  
546 time. Figure 10c is a good illustration of this phenomenon, showing the augmentation of the relative part  
547 of streamflow uncertainty when increasing the sample size.

548 The maxpost values of the 205 years sample is higher than the 100 and 150 years samples (figure 10b),  
549 probably because of the inclusion of the two largest floods of the history in the 205 years sample (1840  
550 and 1856 floods). Thus, without using those old hydrometric data (1816-1870), the 1000-year flood could  
551 have been 15% lower in this specific case. Figure 10d shows that the streamflow uncertainty has a minor  
552 impact on shape parameter uncertainty compared with the sampling uncertainty. The sample size impact  
553 on flood quantiles estimation is further explored in Figure 10e. The 1000-year flood (maxpost) and the  
554 relative contributions of both sources of uncertainty are estimated for several sample sizes, from 20 to 205  
555 years, with a two-year step. A large reduction of sampling uncertainty (and of the total uncertainty as a  
556 consequence) appears between 20 and 100 years, along with the reduction of the maxpost value. Then, the  
557 maxpost and uncertainty intervals are constant between 100 and 160 years of sample size, until the inclusion  
558 of 1856 and 1840 major floods that lead to a slight increase in the estimated quantile. The total uncertainty  
559 interval width is not much changed by those flood inclusions but the relative contribution of streamflow  
560 uncertainty is larger.

## 561 5 Discussion

### 562 5.1 Usefulness of disentangling the various sources of uncertainty in FFA

563 Even though sampling uncertainty is a major concern in FFA, historical continuous stage records are  
564 rarely used. The laborious process of gathering and reanalyzing data, and concerns about the reliability of  
565 the resulting discharge series may be the potential reasons for this oversight. Moreover, the estimation and  
566 the propagation of the various sources of uncertainty throughout the FFA chain is not straightforward to  
567 achieve. Several papers performed an integrated analysis in which both rating curve parameters and flood  
568 frequency distribution were estimated (Petersen-Øverleir and Reitan (2009); Steinbakk et al. (2016); Vieira  
569 et al. (2022)). They concluded that accounting for rating curve uncertainties may notably widen the total  
570 uncertainty of flood quantiles. More specifically, Steinbakk et al. (2016) based their case study on several  
571 Norwegian rivers, with sample sizes up to 100 years. They found that sampling uncertainty is generally the  
572 main contributor (i.e. versus rating curve uncertainty) to design flood estimates and that its contribution  
573 decreases when sample size increases.

574 The approach proposed in this paper does not only consider rating curve uncertainty, but also stage  
575 uncertainties (that combine stage measurement and time interpolation errors) and rating changes. Their  
576 consideration is crucial when dealing with long streamflow series. The case study investigated in this paper  
577 is based on a 205-year long continuous sample, which enables an in-depth evaluation of the contribution of  
578 the different sources of uncertainty in design flood estimates ~~for usual and longer than unusual sample sizes~~  
579 ~~from series of several decades to long series exceeding one century of systematic record~~. The results show  
580 that the estimated 95% streamflow uncertainty is not negligible and varies from 30% (XIX<sup>th</sup> Century) to  
581 5% (1967-2020). The larger streamflow uncertainty of the XIX<sup>th</sup> Century is mostly due to stage uncertainty,  
582 which emphasises the importance of paying a particular attention to this uncertainty source when using  
583 historical stage measurements. Streamflow uncertainty is then propagated to flood quantiles estimates. For  
584 the 205-year long flood sample, streamflow uncertainty dominates for return periods below 100 years but  
585 sampling uncertainty becomes dominant when the return period tends toward 1000 years. The 205-year long  
586 streamflow series enables exploring the contribution of streamflow and sampling uncertainties for various  
587 sample sizes. Sampling uncertainty contribution decreases when sample size increases, unlike streamflow  
588 uncertainty contribution which increases when older data are included. Although the relative contribution  
589 of each source of uncertainty on extreme quantiles varies, the width of the total uncertainty interval does not  
590 change much from 100 to 205 years samples. Nevertheless, in this case study, the maxpost value of extreme  
591 quantiles is increased by 15% when considering 205 years rather than 150 or 100 years, as the two largest  
592 floods since 1816 occurred during the first 40 years of records. This emphasizes that using longer records  
593 does not only affect the uncertainty around flood quantiles, but also the value of the quantiles themselves.

## 594 5.2 Potential improvements of the method and further analyses

595 The streamflow uncertainty analysis procedure proposed in this work is affected by several limitations.  
596 The gauging segmentation model proposed by Darienzo et al. (2021) (or more generally any gaugings-based  
597 segmentation approach) is limited when gaugings are scarce. Some rating shifts are likely to be missed, and  
598 even when one is detected, assigning a precise shift time is difficult when very little information is available  
599 about rating changes and channel morphology. Other approaches could be trialed to detect changes in the  
600 stage-discharge relationship, such as the analysis of stage or discharge recessions (for instance: Nathan and  
601 McMahon (1990); Tallaksen (1995); Vogel and Kroll (1996); Chapman (1999); Lang et al. (2010); Darienzo  
602 (2021)) or the occurrences of morphogenic events (Darienzo (2021)).

603 Another limitation of the method comes from the elicitation of hydraulic priors in a historical context, for  
604 which information about hydraulic configurations is scarce. This lack of knowledge is particularly detrimental  
605 for stations where changes in bed morphology are frequent. As described by Petersen-Øverleir and Reitan

606 (2009), the extrapolation of rating curves in this context is more uncertain, thus affecting flood quantile  
607 estimates.

608 The shape parameter is of great importance as it determines the tail behaviour of the GEV distribution.  
609 Several regional or local-regional methods have been proposed to reduce the uncertainty of the shape pa-  
610 rameter estimation (Burn (1990); Ouarda et al. (2001); Ribatet et al. (2007); Micevski and Kuczera (2009);  
611 Haddad and Rahman (2012)). This could be a source of improvement, but a regional approach could be  
612 difficult to apply here, because catchments as large as the Rhône River at Beaucaire cover many different  
613 climatic influences and are quite unique, which makes the use of other similar catchments challenging. An  
614 alternative solution to this approach is to analyse floods in the main subcatchments and their concomitance.

615 The underlying assumption of stationarity required for FFA is questionable due to anthropogenic climate  
616 change, as described by Milly et al. (2008). However, Madsen et al. (2014) underlined that no particular  
617 guideline for climate change adjustment factors on design flood are given in France. Trends in flood magni-  
618 tudes have been identified in several climatic regions of Europe (Hall et al. (2014); Blöschl et al. (2019)) and  
619 France (Giuntoli et al., 2019), but not everywhere and with large regional differences. Many approaches of  
620 FFA accounting for non-stationarity have emerged (as reviewed by Salas et al. (2018)) and are sometimes  
621 combined with regional approaches (Han et al., 2022). After identifying the regional trends of the Rhône  
622 River, a next challenge could be to develop a climate-informed model to account for the effects of climate  
623 change on floods.

624 Finally, a promising development is to use **sporadic** flood evidences older than systematic stage mea-  
625 surements. **This data can come from various origins such as testimonies (Pichard and Roucaute, 2014),**  
626 **flood marks (Renard, 2023), paleoflood evidences based on slack water deposits (Sheffer et al., 2003), lake**  
627 **sediments (Wilhelm et al., 2022) or sediments within the Rhone prodelta (Fanget et al., 2013).** Various  
628 procedures have been developed in the literature **to include such data in FFA** through the use of perception  
629 threshold and censored data **as summarized by** (Brázil et al., 2006; Kjeldsen et al., 2014; England et al.,  
630 2019; Harden et al., 2021). Such approaches have been applied in Europe, including France (Naulet et al.  
631 (2005); Lang et al. (2010); Neppel et al. (2010); Payrastre et al. (2011)) and could be interesting for the  
632 Lower-Rhône Valley for which many flood evidences (along with information on other climate-related dis-  
633 asters) have been gathered. Pichard and Roucaute (2014) and Pichard et al. (2017) have identified more  
634 than 1500 hydro-climatic events in the Lower-Rhône Valley since the XIV<sup>th</sup> Century, synthesized in the  
635 HISTRHÔNE database ([histrhone.cerege.fr](http://histrhone.cerege.fr)). The flood events are classified by magnitude of damages,  
636 and further investigations are required to identify the perception thresholds corresponding to those different

637 magnitudes. In addition, as this information is not exhaustive (unlike the stage measurements used in this  
638 paper), the extension of the sample before 1816 requires a different statistical treatment. Moreover, the  
639 interest of long discharge series and flood evidences is not limited to standard FFA, but is also useful for  
640 studying the long-term historical variability of floods (e.g Macdonald and Sangster, 2017).

### 641 5.3 Are historical stage records useful for flood frequency analysis?

642 The interest of including historical stage records to reduce sampling uncertainty in FFA should be balanced  
643 against the large streamflow uncertainty induced by those records. For the specific case of Beaucaire, the  
644 use of historical stage records is clearly beneficial up to a 100-year sample size, but the added value is not  
645 as clear with longer samples (see section 4.5.3 and figure 10). Evaluating the procedure on more stations  
646 with historical systematic stage records would be necessary in order to generalize the results. The respective  
647 contribution of streamflow and sampling uncertainties could be different for other stations depending on  
648 their respective hydraulic configuration and river bed stability.

649 In this paper, the estimation of flood discharges follows the usual hydrometric process (i.e. converting  
650 the measured stages into discharges via the estimation of rating curves from gaugings). However, the stage  
651 measurements and gaugings from the XIX<sup>th</sup> Century are scarce compared to recent decades, which leads to  
652 large uncertainties around flood discharges. Those uncertainties could be reduced in multiple ways, including  
653 the use of hydraulic models. This practice is widespread in the literature and is generally applied to floods  
654 older than systematic measurements (for instance: Naulet et al. (2005); Neppel et al. (2010); Machado  
655 et al. (2015); Ruiz-Bellet et al. (2017); Van der Meulen et al. (2021)). Yet, it requires topographic and  
656 bathymetric data that may be even more scarce and uncertain than gaugings. Moreover, the use of flood  
657 evidences older than systematic measurements generally leads to the assumption that all the floods greater  
658 than an identified perception threshold are known, as well as the magnitude of the threshold itself.

659 The specific conclusions of the Rhône River at Beaucaire may not be generalized to other climatic regions  
660 for which the tail behaviour of flood distribution is influenced by different processes (Merz et al., 2022).  
661 More specifically, the Rhône River at Beaucaire has a positive shape parameter, which corresponds to a  
662 light-tailed behavior with the GEV parameterization used in this paper. While this might be typical of such  
663 large catchments, many smaller catchments display the opposite heavy-tailed behavior. Whether or not the  
664 main conclusions drawn in this paper would still hold with such smaller catchments remains to be evaluated.

666 **6 Conclusion**

667 Flood hazard estimation is affected by several sources of uncertainty, including sampling uncertainty that  
668 is dominant for usual sample sizes (less than 100 years). It is sometimes possible to gather historical continu-  
669 ous stage measurements in order to enlarge flood samples beyond usual sizes. This process has the potential  
670 to reduce the uncertainties of design flood estimates. Nevertheless, the streamflow series derived from these  
671 historical stage series are generally affected by much greater uncertainties than modern series. This paper  
672 investigates the following questions: to what extent does including historical (and thus uncertain) hydro-  
673 metric data improves FFA estimates, and what is the contribution of streamflow and sampling uncertainties  
674 to the total FFA uncertainty ? Those questions are explored through a general FFA framework accounting  
675 for the specific uncertainties affecting long hydrometric series. This uncertainty propagation chain is applied  
676 to a 205-year long continuous stage series of the Rhône River at Beaucaire.

677 The estimated streamflow uncertainty varies from 30% (XIX<sup>th</sup> Century) to 5% (1967-2020). This uncer-  
678 tainty is propagated to flood quantiles estimates. When using the full flood sample (205 years), streamflow  
679 uncertainty is dominant below the 100-year flood and sampling uncertainty is dominant above. However,  
680 this conclusion is sensitive to the available sample size. The sample size impact on design flood estimates  
681 is explored by subsampling the full flood sample. The total uncertainty of flood quantiles substantially  
682 decreases from 20- to 100-year samples. This decrease is directly induced by the reduction of sampling  
683 uncertainty. For sample sizes between 100 and 205 years, the total uncertainty is nearly constant because  
684 the sampling uncertainty reduction is offset by the increase of streamflow uncertainty (older flood discharges  
685 are more uncertain). However, the central flood quantiles estimates increase by about 15% when increasing  
686 sample size between 160 and 205 years, because of the inclusion of the two largest floods that occurred  
687 during the first 40 years of measurement. Yet, this 15% increase is slight with respect to the total uncer-  
688 tainty. One should be cautious about generalizing these results beyond the particular case of the Rhône  
689 River at Beaucaire, as the contribution of sampling and streamflow uncertainties may strongly depend on  
690 the properties of the station and the catchment.

691 Finally, this article promotes the use of historical stage records to improve design flood estimates and  
692 underline the particular importance of estimating and propagating all sources of uncertainty through the  
693 estimation process. Discussions are currently underway with the competent authorities in flood risk man-  
694 agement concerning the updating of design flood (Q100, Q1000, Q1500) with enlarged samples (from 80 to  
695 205 year-discharge series), and on ways to account for estimation uncertainty. The use of estimates derived  
696 from the predictive distribution (also referred to as the expected probability approach, e.g. Kuczera, 1999;

697 Renard et al., 2013) could be considered since it is naturally suited to the Bayesian approach used here.  
698 Interesting improvements may come from the use of **sporadic** flood evidences older than the systematic stage  
699 measurements used in this paper, or from regional or nonstationary FFA approaches. Moreover, beyond  
700 standard FFA, such long series also have the potential to shed light on the long-term historical variability  
701 of floods.

## 7 Acknowledgements

702 The PhD fellowship of Mathieu Lucas is funded by INRAE, the Compagnie Nationale du Rhône (CNR)  
703 and EUR H2O'Lyon (ANR-17-EURE-0018) from the University of Lyon. This study was conducted within  
704 the Rhône Sediment Observatory (OSR), a multi-partner research program funded through the Plan Rhône  
705 by the European Regional Development Fund (ERDF), Agence de l'eau RMC, CNR, EDF, and three regional  
706 councils (Auvergne-Rhône-Alpes, PACA, and Occitanie). Data and expert knowledge on the Rhône River  
707 at Beaucaire were provided by CNR, the Rhône Sediment Observatory, Pascal Billy and Helene Decourcelle  
708 from the DREAL Auvergne-Rhône-Alpes (Ministry of Ecology) and the HISTRHONE database from the  
709 CEREGE (Georges Pichard).

711 –The uncertainty propagation code is available at <https://github.com/MatLcs/PropagMaxAn> and the  
712 data is available at <https://www.plan-rhone.fr/>

713 The data is available at <https://www.plan-rhone.fr/> (up to 2016) and uncertainty propagation code with  
714 the whole data set ("QuantilesAmax.txt") is available at <https://github.com/MatLcs/PropagMaxAn>.

## 715 References

- 716 Armand (1907). "II. Le Rhône à Tarascon (Planche I)". In: Revue des Études Anciennes 9.1, pp. 19–21.  
717 ISSN: 0035-2004. DOI: [10.3406/rea.1907.1469](https://doi.org/10.3406/rea.1907.1469).
- 718 Bard, A. and M. Lang (2018). Actualisation de l'hydrologie des crues du Rhône. Analyse de la station de Beaucairn  
719 Irstea pour la DREAL Auvergne-Rhône-Alpes, p. 56.
- 720 Blöschl, G., J. Hall, A. Viglione, R. A. P. Perdigão, J. Parajka, B. Merz, D. Lun, B. Arheimer, G. T. Aronica,  
721 A. Bilibashi, M. Boháč, O. Bonacci, M. Borga, I. Čanjevac, A. Castellarin, G. B. Chirico, P. Claps, N.  
722 Frolova, D. Ganora, L. Gorbachova, A. Gül, J. Hannaford, S. Harrigan, M. Kireeva, A. Kiss, T. R.  
723 Kjeldsen, S. Kohnová, J. J. Koskela, O. Ledvinka, N. Macdonald, M. Mavrova-Guirguinova, L. Mediero,  
724 R. Merz, P. Molnar, A. Montanari, C. Murphy, M. Osuch, V. Ovcharuk, I. Radevski, J. L. Salinas, E.  
725 Sauquet, M. Šraj, J. Szolgay, E. Volpi, D. Wilson, K. Zaimi, and N. Živković (2019). "Changing climate

- 726 both increases and decreases European river floods". In: Nature 573.7772, pp. 108–111. ISSN: 1476-4687.  
727 DOI: [10.1038/s41586-019-1495-6](https://doi.org/10.1038/s41586-019-1495-6).
- 728 Brázdil, R., Z. W. Kundzewicz, and G. Benito (2006). "Historical hydrology for studying flood risk in  
729 Europe". In: Hydrological Sciences Journal 51.5, pp. 739–764. ISSN: 0262-6667, 2150-3435. DOI: [10.1623/hysj.51.5.739](https://doi.org/10.1623/hysj.51.5.739).
- 730 Burn, D. H. (1990). "Evaluation of regional flood frequency analysis with a region of influence approach".  
731 In: Water Resources Research 26.10, pp. 2257–2265. ISSN: 1944-7973. DOI: [10.1029/WR026i010p02257](https://doi.org/10.1029/WR026i010p02257).
- 732 CETIAT (2005). Conférence de consensus sur le débit du Rhône à Beaucaire pour la crue de Décembre 2003. An  
733 pour le compte de la CNR. Estimation des incertitudes des débits calculés à partir des relations hau-  
734 teur/débit.
- 735 Chapman, T. (1999). "A comparison of algorithms for stream flow recession and baseflow separation". In:  
736 Hydrological Processes 13.5, pp. 701–714. ISSN: 1099-1085. DOI: [10.1002/\(SICI\)1099-1085\(19990415\)13:5<701::AID-HYP774>3.0.CO;2-2](https://doi.org/10.1002/(SICI)1099-1085(19990415)13:5<701::AID-HYP774>3.0.CO;2-2).
- 737 Coles, S. (2001). "Classical Extreme Value Theory and Models". In: An Introduction to Statistical Modeling of Extremes  
738 Ed. by S. Coles. Springer Series in Statistics. London: Springer, pp. 45–73. ISBN: 978-1-4471-3675-0. DOI:  
739 [10.1007/978-1-4471-3675-0\\_3](https://doi.org/10.1007/978-1-4471-3675-0_3).
- 740 Coxon, G., J. Freer, I. K. Westerberg, T. Wagener, R. Woods, and P. J. Smith (2015). "A novel framework for  
741 discharge uncertainty quantification applied to 500 UK gauging stations". In: Water Resources Research  
742 51.7, pp. 5531–5546. ISSN: 0043-1397, 1944-7973. DOI: [10.1002/2014WR016532](https://doi.org/10.1002/2014WR016532).
- 743 Darienzo, M., B. Renard, J. Le Coz, and M. Lang (2021). "Detection of Stage-Discharge Rating Shifts Using  
744 Gaugings: A Recursive Segmentation Procedure Accounting for Observational and Model Uncertainties".  
745 In: Water Resources Research 57.4. ISSN: 0043-1397, 1944-7973. DOI: [10.1029/2020WR028607](https://doi.org/10.1029/2020WR028607).
- 746 Darienzo, M. (2021). "Detection and estimation of stage-discharge rating shifts for retrospective and real-  
747 time streamflow quantification". These de doctorat. Université Grenoble Alpes.
- 748 Dymond, J. R. and R. Christian (1982). "Accuracy of discharge determined from a rating curve". In:  
749 Hydrological Sciences Journal 27.4, pp. 493–504. ISSN: 0262-6667, 2150-3435. DOI: [10.1080/0262666820949112](https://doi.org/10.1080/0262666820949112).
- 750 England, J. F. J., T. A. Cohn, B. A. Faber, J. R. Stedinger, W. O. T. Jr, A. G. Veilleux, J. E. Kiang, and  
751 J. Robert R. Mason (2019). Guidelines for determining flood flow frequency — Bulletin 17C. 4-B5. U.S.  
752 Geological Survey.
- 753 Fanget, A.-S., M.-A. Bassetti, M. Arnaud, J.-F. Chiffolleau, D. Cossa, A. Goineau, C. Fontanier, R. Buscail,  
754 G. Jouet, G. Maillet, A. Negri, B. Dennielou, and S. Berné (2013). "Historical evolution and extreme  
755 climate events during the last 400years on the Rhone prodelta (NW Mediterranean)". In: Marine Geology  
756 346, pp. 375–391. ISSN: 00253227. DOI: [10.1016/j.margeo.2012.02.007](https://doi.org/10.1016/j.margeo.2012.02.007).

- 759 Giuntoli, I., B. Renard, and M. Lang (2019). “Floods in France”. In: Changes in Flood Risk in Europe.  
760 1st ed. CRC Press, p. 13. ISBN: 978-0-203-09809-7.
- 761 Guerrero, J.-L., I. K. Westerberg, S. Halldin, C.-Y. Xu, and L.-C. Lundin (2012). “Temporal variability  
762 in stage–discharge relationships”. In: Journal of Hydrology 446-447, pp. 90–102. ISSN: 00221694. DOI:  
763 [10.1016/j.jhydrol.2012.04.031](https://doi.org/10.1016/j.jhydrol.2012.04.031).
- 764 Haddad, K. and A. Rahman (2012). “Regional flood frequency analysis in eastern Australia: Bayesian GLS  
765 regression-based methods within fixed region and ROI framework – Quantile Regression vs. Parameter  
766 Regression Technique”. In: Journal of Hydrology 430-431, pp. 142–161. ISSN: 0022-1694. DOI: [10.1016/j.jhydrol.2012.02.012](https://doi.org/10.1016/j.jhydrol.2012.02.012).
- 767 Hall, J., B. Arheimer, M. Borga, R. Brázil, P. Claps, A. Kiss, T. R. Kjeldsen, J. Kriauciūnienė, Z. W.  
768 Kundzewicz, M. Lang, M. C. Llasat, N. Macdonald, N. McIntyre, L. Mediero, B. Merz, R. Merz, P. Mol-  
769 nar, A. Montanari, C. Neuhold, J. Parajka, R. A. P. Perdigão, L. Plavcová, M. Rogger, J. L. Salinas, E.  
770 Sauquet, C. Schär, J. Szolgay, A. Viglione, and G. Blöschl (2014). “Understanding flood regime changes  
771 in Europe: a state-of-the-art assessment”. In: Hydrology and Earth System Sciences 18.7, pp. 2735–2772.  
772 ISSN: 1607-7938. DOI: [10.5194/hess-18-2735-2014](https://doi.org/10.5194/hess-18-2735-2014).
- 773 Hamed, K. H. and A. Ramachandra Rao (2019). Flood Frequency Analysis. 1st ed. CRC Press. ISBN: 978-  
774 0-429-12881-3. DOI: [10.1201/9780429128813](https://doi.org/10.1201/9780429128813).
- 775 Hamilton, A. and R. Moore (2012). “Quantifying Uncertainty in Streamflow Records”. In: Canadian Water Resources  
776 37.1, pp. 3–21. ISSN: 0701-1784, 1918-1817. DOI: [10.4296/cwrj3701865](https://doi.org/10.4296/cwrj3701865).
- 777 Han, X., R. Mehrotra, A. Sharma, and A. Rahman (2022). “Incorporating nonstationarity in regional flood  
778 frequency analysis procedures to account for climate change impact”. In: Journal of Hydrology 612,  
779 p. 128235. ISSN: 0022-1694. DOI: [10.1016/j.jhydrol.2022.128235](https://doi.org/10.1016/j.jhydrol.2022.128235).
- 780 Harden, T. M., K. R. Ryberg, J. E. O’Connor, J. M. Friedman, and J. E. Kiang (2021). Historical and paleoflood anal-  
781 4-B6. ISSN: 2328-7055 Publication Title: Techniques and Methods. U.S. Geological Survey. DOI: [10.3133/tm4B6](https://doi.org/10.3133/tm4B6).
- 782 Herschy, R. (1998). Hydrometry Principles and Practices. 2nd ed. John Wiley. 384 pp.
- 783 Horner, I., B. Renard, J. Le Coz, F. Branger, H. K. McMillan, and G. Pierrefeu (2018). “Impact of Stage  
784 Measurement Errors on Streamflow Uncertainty”. In: Water Resources Research 54.3, pp. 1952–1976.  
785 ISSN: 0043-1397, 1944-7973. DOI: [10.1002/2017WR022039](https://doi.org/10.1002/2017WR022039).
- 786 Ibbitt, R. P. and C. P. Pearson (1987). “Gauging frequency and detection of rating changes”. In: Hydrological Scienc-  
787 32.1, pp. 85–103. ISSN: 0262-6667, 2150-3435. DOI: [10.1080/02626668709491164](https://doi.org/10.1080/02626668709491164).
- 788 Jain, S. K. and V. P. Singh (2019). “Design Flood Estimation”. In: Engineering Hydrology: An Introduction to Pro-  
789 First edition. New York: McGraw-Hill Education. ISBN: 978-1-259-64197-8.

- 792 Juston, J., P.-E. Jansson, and D. Gustafsson (2014). "Rating curve uncertainty and change detection in  
793 discharge time series: case study with 44-year historic data from the Nyangores River, Kenya". In:  
794 *Hydrological Processes* 28.4, pp. 2509–2523. ISSN: 08856087. DOI: [10.1002/hyp.9786](https://doi.org/10.1002/hyp.9786).
- 795 Kendall, M. (1948). *Rank Correlation Methods*. 1. London: Charles Griffin & Company.
- 796 Kiang, J. E., C. Gazoorian, H. McMillan, G. Coxon, J. L. Coz, I. K. Westerberg, A. Belleville, D. Sevrez, A. E.  
797 Sikorska, A. Petersen-Øverleir, T. Reitan, J. Freer, B. Renard, V. Mansanarez, and R. Mason (2018). "A  
798 Comparison of Methods for Streamflow Uncertainty Estimation". In: *Water Resources Research* 54.10,  
799 pp. 7149–7176. DOI: <https://doi.org/10.1029/2018WR022708>.
- 800 Kjeldsen, T., N. Macdonald, M. Lang, L. Mediero, T. Albuquerque, E. Bogdanowicz, R. Brázdil, A. Castel-  
801 larin, V. David, A. Fleig, G. Gül, J. Kriauciuniene, S. Kohnová, B. Merz, O. Nicholson, L. Roald,  
802 J. Salinas, D. Sarauskiene, M. Šraj, W. Strupczewski, J. Szolgay, A. Toumazis, W. Vanneuville, N.  
803 Veijalainen, and D. Wilson (2014). "Documentary evidence of past floods in Europe and their util-  
804 ity in flood frequency estimation". In: *Journal of Hydrology* 517, pp. 963–973. ISSN: 00221694. DOI:  
805 [10.1016/j.jhydrol.2014.06.038](https://doi.org/10.1016/j.jhydrol.2014.06.038).
- 806 Kjeldsen, T. R., R. Lamb, and S. D. Blazkova (2011). "Uncertainty in Flood Frequency Analysis". In:  
807 *Applied Uncertainty Analysis for Flood Risk Management*. Imperial college press, pp. 153–197. ISBN:  
808 978-1-84816-270-9.
- 809 Kuczera, G. (1999). "Comprehensive at-site flood frequency analysis using Monte Carlo Bayesian inference".  
810 In: *Water Resources Research* 35.5, pp. 1551–1557. ISSN: 1944-7973. DOI: [10.1029/1999WR900012](https://doi.org/10.1029/1999WR900012).
- 811 Kuentz, A., T. Mathevret, D. Cœur, C. Perret, J. Gailhard, L. Guérin, Y. Gash, and V. Andréassian (2014).  
812 "Hydrométrie et hydrologie historiques du bassin de la Durance". In: *La Houille Blanche* 100.4, pp. 57–  
813 63. ISSN: 0018-6368, 1958-5551. DOI: [10.1051/lhb/2014039](https://doi.org/10.1051/lhb/2014039).
- 814 Lang, M. and D. Coeur (2014). *Les inondations remarquables en France. Inventaire 2011 pour la directive Inondation*  
815 1st ed. Hors Collection. Editions Quae. 640 pp. ISBN: 978-2-7592-2260-5.
- 816 Lang, M., K. Pobanz, B. Renard, E. Renouf, and E. Sauquet (2010). "Extrapolation of rating curves by  
817 hydraulic modelling, with application to flood frequency analysis". In: *Hydrological Sciences Journal*  
818 55.6, pp. 883–898. ISSN: 0262-6667, 2150-3435. DOI: [10.1080/02626667.2010.504186](https://doi.org/10.1080/02626667.2010.504186).
- 819 Łapuszek, M. and A. Lenar-Matyas (2015). "Methods of analysis the riverbed evolution. a case study of two  
820 tributaries of the upper Vistula river". In: *Infrastruktura i Ekologia Terenów Wiejskich / Infrastructure and ec-*  
821 *(IV/3/2015)*, pp. 1313–1327. ISSN: 1732-5587. DOI: [10.14597/infraeco.2015.4.3.095](https://doi.org/10.14597/infraeco.2015.4.3.095).
- 822 Le Coz, J., P.-M. Bechon, B. Camenen, and G. Dramais (2014a). "Quantification des incertitudes sur les  
823 jaugeages par exploration du champ des vitesses". In: *La Houille Blanche* 100.5, pp. 31–39. ISSN: 0018-  
824 6368, 1958-5551. DOI: [10.1051/lhb/2014047](https://doi.org/10.1051/lhb/2014047).

- 825 Le Coz, J., B. Renard, L. Bonnifait, F. Branger, and R. Le Boursicaud (2014b). “Combining hydraulic  
826 knowledge and uncertain gaugings in the estimation of hydrometric rating curves: A Bayesian approach”.  
827 In: *Journal of Hydrology* 509, pp. 573–587. ISSN: 00221694. DOI: [10.1016/j.jhydrol.2013.11.016](https://doi.org/10.1016/j.jhydrol.2013.11.016).
- 828 Le Delliou, P. (2014). “Recommandations pour le dimensionnement des évacuateurs de crues de barrages”.  
829 In: *La Houille Blanche* 100.5, pp. 54–58. ISSN: 0018-6368, 1958-5551. DOI: [10.1051/lhb/2014050](https://doi.org/10.1051/lhb/2014050).
- 830 Macdonald, N. and H. Sangster (2017). “High-magnitude flooding across Britain since AD 1750”. In:  
831 *Hydrology and Earth System Sciences* 21.3. Publisher: Copernicus GmbH, pp. 1631–1650. ISSN: 1027-  
832 5606. DOI: [10.5194/hess-21-1631-2017](https://doi.org/10.5194/hess-21-1631-2017).
- 833 Machado, M. J., B. A. Botero, J. López, F. Francés, A. Díez-Herrero, and G. Benito (2015). “Flood frequency  
834 analysis of historical flood data under stationary and non-stationary modelling”. In: *Hydrology and Earth System  
835 Sciences* 19.6, pp. 2561–2576. ISSN: 1607-7938. DOI: [10.5194/hess-19-2561-2015](https://doi.org/10.5194/hess-19-2561-2015).
- 836 Madsen, H., D. Lawrence, M. Lang, M. Martinkova, and T. R. Kjeldsen (2014). “Review of trend analysis  
837 and climate change projections of extreme precipitation and floods in Europe”. In: *Journal of Hydrology  
838* 519, pp. 3634–3650. ISSN: 0022-1694. DOI: [10.1016/j.jhydrol.2014.11.003](https://doi.org/10.1016/j.jhydrol.2014.11.003).
- 839 Mann, H. B. (1945). “Nonparametric Tests Against Trend”. In: *Econometrica* 13.3. Publisher: [Wiley, Econo-  
840 metric Society], pp. 245–259. ISSN: 0012-9682. DOI: [10.2307/1907187](https://doi.org/10.2307/1907187).
- 841 Mansanarez, V., B. Renard, J. L. Coz, M. Lang, and M. Darienzo (2019a). “Shift Happens! Adjusting Stage-  
842 Discharge Rating Curves to Morphological Changes at Known Times”. In: *Water Resources Research  
843* 55.4, pp. 2876–2899. ISSN: 0043-1397, 1944-7973. DOI: [10.1029/2018WR023389](https://doi.org/10.1029/2018WR023389).
- 844 Mansanarez, V. (2016). “Non-unique stage-discharge relations : Bayesian analysis of complex rating curves  
845 and their uncertainties”. PhD thesis. Université Grenoble Alpes.
- 846 Mansanarez, V., I. K. Westerberg, N. Lam, and S. W. Lyon (2019b). “Rapid Stage-Discharge Rating Curve  
847 Assessment Using Hydraulic Modeling in an Uncertainty Framework”. In: *Water Resources Research  
848* 55.11, pp. 9765–9787. ISSN: 0043-1397, 1944-7973. DOI: [10.1029/2018WR024176](https://doi.org/10.1029/2018WR024176).
- 849 Martins, E. S. and J. R. Stedinger (2000). “Generalized maximum-likelihood generalized extreme-value  
850 quantile estimators for hydrologic data”. In: *Water Resources Research* 36.3, pp. 737–744. ISSN: 00431397.  
851 DOI: [10.1029/1999WR900330](https://doi.org/10.1029/1999WR900330).
- 852 McMillan, H. K. and I. K. Westerberg (2015). “Rating curve estimation under epistemic uncertainty”. In:  
853 *Hydrological Processes* 29.7, pp. 1873–1882. ISSN: 08856087. DOI: [10.1002/hyp.10419](https://doi.org/10.1002/hyp.10419).
- 854 McMillan, H., J. Freer, F. Pappenberger, T. Krueger, and M. Clark (2010). “Impacts of uncertain river flow  
855 data on rainfall-runoff model calibration and discharge predictions”. In: 24. DOI: <https://doi.org/10.1002/hyp.7587>.

- 857 McMillan, H., T. Krueger, and J. Freer (2012). "Benchmarking observational uncertainties for hydrology: rainfall, river discharge and water quality". In: *Hydrological Processes* 26.26, pp. 4078–4111. ISSN: 858 08856087. DOI: [10.1002/hyp.9384](https://doi.org/10.1002/hyp.9384).
- 860 MEDD (2005). *Débit du Rhône à Beaucaire pour la crue de Décembre 2003*. Conférence de consensus. Minitère 861 français de l'écologie et du développement durable.
- 862 Merz, B., S. Basso, S. Fischer, D. Lun, G. Blöschl, R. Merz, B. Guse, A. Viglione, S. Vorogushyn, E. Mac- 863 donald, L. Wietzke, and A. Schumann (2022). "Understanding Heavy Tails of Flood Peak Distributions". 864 In: *Water Resources Research* 58.6, e2021WR030506. ISSN: 1944-7973. DOI: [10.1029/2021WR030506](https://doi.org/10.1029/2021WR030506).
- 865 Micevski, T. and G. Kuczera (2009). "Combining site and regional flood information using a Bayesian Monte 866 Carlo approach". In: *Water Resources Research* 45.4. ISSN: 1944-7973. DOI: [10.1029/2008WR007173](https://doi.org/10.1029/2008WR007173).
- 867 Milly, P. C. D., J. Betancourt, M. Falkenmark, R. M. Hirsch, Z. W. Kundzewicz, D. P. Lettenmaier, and R. J. 868 Stouffer (2008). "Stationarity Is Dead: Whither Water Management?" In: *Science* 319.5863, pp. 573–574. 869 ISSN: 0036-8075, 1095-9203. DOI: [10.1126/science.1151915](https://doi.org/10.1126/science.1151915).
- 870 Morlot, T., C. Perret, A.-C. Favre, and J. Jalbert (2014). "Dynamic rating curve assessment for hydrometric 871 stations and computation of the associated uncertainties: Quality and station management indicators". 872 In: *Journal of Hydrology* 517, pp. 173–186. ISSN: 00221694. DOI: [10.1016/j.jhydrol.2014.05.007](https://doi.org/10.1016/j.jhydrol.2014.05.007).
- 873 Nathan, R. J. and T. A. McMahon (1990). "Evaluation of automated techniques for base flow and re- 874 cession analyses". In: *Water Resources Research* 26.7, pp. 1465–1473. ISSN: 1944-7973. DOI: [10.1029/WR026i007p01465](https://doi.org/10.1029/WR026i007p01465).
- 875 Naulet, R., M. Lang, T. B. Ouarda, D. Coeur, B. Bobée, A. Recking, and D. Moussay (2005). "Flood 876 frequency analysis on the Ardèche river using French documentary sources from the last two centuries". 877 In: *Journal of Hydrology* 313.1, pp. 58–78. ISSN: 00221694. DOI: [10.1016/j.jhydrol.2005.02.011](https://doi.org/10.1016/j.jhydrol.2005.02.011).
- 878 Neppel, L., B. Renard, M. Lang, P.-A. Ayral, D. Coeur, E. Gaume, N. Jacob, O. Payrastre, K. Pobanz, and 879 F. Vinet (2010). "Flood frequency analysis using historical data: accounting for random and systematic 880 errors". In: *Hydrological Sciences Journal* 55.2, pp. 192–208. ISSN: 0262-6667, 2150-3435. DOI: [10.1080/02626660903546092](https://doi.org/10.1080/02626660903546092).
- 881 Ouarda, T. B. M. J., C. Girard, G. S. Cavadias, and B. Bobée (2001). "Regional flood frequency estimation 882 with canonical correlation analysis". In: *Journal of Hydrology* 254.1, pp. 157–173. ISSN: 0022-1694. DOI: 883 [10.1016/S0022-1694\(01\)00488-7](https://doi.org/10.1016/S0022-1694(01)00488-7).
- 884 Payrastre, O., E. Gaume, and H. Andrieu (2011). "Usefulness of historical information for flood frequency 885 analyses: Developments based on a case study". In: *Water Resources Research* 47.8. ISSN: 00431397. DOI: 886 [10.1029/2010WR009812](https://doi.org/10.1029/2010WR009812).

- 889 Petersen-Øverleir, A. and T. Reitan (2005). "Uncertainty in flood discharges from urban and small rural  
890 catchments due to inaccurate head measurement". In: Hydrology Research 36.3, pp. 245–257. ISSN: 0029-  
891 1277, 2224-7955. DOI: [10.2166/nh.2005.0018](https://doi.org/10.2166/nh.2005.0018).
- 892 Petersen-Øverleir, A. and T. Reitan (2009). "Accounting for rating curve imprecision in flood frequency  
893 analysis using likelihood-based methods". In: Journal of Hydrology 366.1, pp. 89–100. ISSN: 00221694.  
894 DOI: [10.1016/j.jhydrol.2008.12.014](https://doi.org/10.1016/j.jhydrol.2008.12.014).
- 895 Petersen-Øverleir, A., A. Soot, and T. Reitan (2009). "Bayesian Rating Curve Inference as a Streamflow  
896 Data Quality Assessment Tool". In: Water Resources Management 23.9, pp. 1835–1842. ISSN: 0920-4741,  
897 1573-1650. DOI: [10.1007/s11269-008-9354-5](https://doi.org/10.1007/s11269-008-9354-5).
- 898 Pichard, G., G. Arnaud-Fassetta, V. Moron, and E. Roucaute (2017). "Hydro-climatology of the Lower  
899 Rhône Valley: historical flood reconstruction (AD 1300–2000) based on documentary and instrumental  
900 sources". In: Hydrological Sciences Journal 62.11, pp. 1772–1795. ISSN: 0262-6667, 2150-3435. DOI: [10.1080/02626667.2017.1349314](https://doi.org/10.1080/02626667.2017.1349314).
- 901 Pichard, G. (2013). Hauteurs et altitudes aux échelles du bas Rhône, p. 48.
- 902 Pichard, G. and E. Roucaute (2014). "Sept siècles d'histoire hydroclimatique du Rhône d'Orange à la mer  
903 (1300-2000). Climat, crues, inondations." In: Presses Universitaires de Provence (Hors-série de la revue  
904 Méditerranée), p. 194. DOI: <https://doi.org/10.4000/geocarrefour.9491>.
- 905 Ponts\&Chaussées (1914). Observations hydrométriques du Rhône à Beaucaire, 1914.
- 906 Puechberty, R., C. Perret, S. P. Pitsch, P. Battaglia, A. Belleville, P. Bompart, G. Chauvel, J. Cousseau, G.  
907 Dramais, G. Glaziou, A. Hauet, S. Helouin, M. Lang, F. Larrarte, J. L. Coz, P. Marchand, P. Moquet, O.  
908 Payrastre, P. Pierrefeu, and G. Rauzy (2017). Charte qualité de l'hydrométrie. Guide de bonnes pratiques.  
909 Ministère de l'environnement, de l'énergie et de la mer, France. 86 pp.
- 910 Rantz, S. E. (1982). Measurement and computation of streamflow. USGS Numbered Series 2175. U.S. G.P.O.
- 911 Renard, B., K. Kochanek, M. Lang, F. Garavaglia, E. Paquet, L. Neppel, K. Najib, J. Carreau, P. Arnaud,  
912 Y. Aubert, F. Borchi, J.-M. Soubeyroux, S. Jourdain, J.-M. Veysseire, E. Sauquet, T. Cipriani, and  
913 A. Auffray (2013). "Data-based comparison of frequency analysis methods: A general framework". In:  
914 Water Resources Research 49.2, pp. 825–843. ISSN: 00431397. DOI: [10.1002/wrcr.20087](https://doi.org/10.1002/wrcr.20087).
- 915 Renard, B. (2023). "Use of a national flood mark database to estimate flood hazard in the distant past".  
916 In: Hydrological Sciences Journal 0 (ja), null. ISSN: 0262-6667. DOI: [10.1080/02626667.2023.2212165](https://doi.org/10.1080/02626667.2023.2212165).
- 917 Ribatet, M., E. Sauquet, J.-M. Grésillon, and T. B. M. J. Ouarda (2007). "A regional Bayesian POT  
918 model for flood frequency analysis". In: Stochastic Environmental Research and Risk Assessment 21.4,  
919 pp. 327–339. ISSN: 1436-3240, 1436-3259. DOI: [10.1007/s00477-006-0068-z](https://doi.org/10.1007/s00477-006-0068-z).

- 921 Rigaudière, P., A. Dekergariou, C. Laroche, N. Caze, J. Brun, J. Laborde, and W. Berolo (2000). Etude globale des crues  
922 Tech. rep. SAFEGE Cetiis and Université de Nice.
- 923 Ruiz-Bellet, J. L., X. Castelltort, J. C. Balasch, and J. Tuset (2017). “Uncertainty of the peak flow recon-  
924 struction of the 1907 flood in the Ebro River in Xerta (NE Iberian Peninsula)”. In: Journal of Hydrology  
925 545, pp. 339–354. ISSN: 00221694. DOI: [10.1016/j.jhydrol.2016.12.041](https://doi.org/10.1016/j.jhydrol.2016.12.041).
- 926 Salas, J. D., J. Obeysekera, and R. M. Vogel (2018). “Techniques for assessing water infrastructure for  
927 nonstationary extreme events: a review”. In: Hydrological Sciences Journal 63.3, pp. 325–352. ISSN: 0262-  
928 6667. DOI: [10.1080/02626667.2018.1426858](https://doi.org/10.1080/02626667.2018.1426858).
- 929 Sheffer, N. A., Y. Enzel, G. Benito, T. Grodek, N. Poart, M. Lang, R. Naulet, and D. Cœur (2003).  
930 “Paleofloods and historical floods of the Ardèche River, France”. In: Water Resources Research 39.12.  
931 ISSN: 1944-7973. DOI: [10.1029/2003WR002468](https://doi.org/10.1029/2003WR002468).
- 932 Steinbakk, G. H., T. L. Thorarinssdottir, T. Reitan, L. Schlichting, S. Hølleland, and K. Engeland (2016).  
933 “Propagation of rating curve uncertainty in design flood estimation”. In: Water Resources Research 52.9,  
934 pp. 6897–6915. ISSN: 00431397. DOI: [10.1002/2015WR018516](https://doi.org/10.1002/2015WR018516).
- 935 SYMADREM (2012). Programme de sécurisation des ouvrages de protection contre les crues du Rhône du barrage  
936 p. 490.
- 937 Tallaksen, L. M. (1995). “A review of baseflow recession analysis”. In: Journal of Hydrology 165.1, pp. 349–  
938 370. ISSN: 0022-1694. DOI: [10.1016/0022-1694\(94\)02540-R](https://doi.org/10.1016/0022-1694(94)02540-R).
- 939 Van Der Made, J. (1982). “Determination of the accuracy of water level observations”. In: IAHS Publications  
940 Proceedings of the Exeter Symposium
- 134, pp. 172–184.
- 941 Van der Meulen, B., A. Bomers, K. M. Cohen, and H. Middelkoop (2021). “Late Holocene flood magnitudes  
942 in the Lower Rhine river valley and upper delta resolved by a two-dimensional hydraulic modelling  
943 approach”. In: Earth Surface Processes and Landforms 46.4, pp. 853–868. ISSN: 0197-9337, 1096-9837.  
944 DOI: [10.1002/esp.5071](https://doi.org/10.1002/esp.5071).
- 945 Vieira, L. M. d. S., J. C. L. Sampaio, V. A. F. Costa, and J. C. Eleutério (2022). “Assessing the effects of  
946 rating curve uncertainty in flood frequency analysis”. In: RBRH 27, e11. ISSN: 2318-0331, 1414-381X.  
947 DOI: [10.1590/2318-0331.272220220012](https://doi.org/10.1590/2318-0331.272220220012).
- 948 Vogel, R. M. and C. N. Kroll (1996). “Estimation of baseflow recession constants”. In: Water Resources Management  
949 10.4, pp. 303–320. ISSN: 1573-1650. DOI: [10.1007/BF00508898](https://doi.org/10.1007/BF00508898).
- 950 Westerberg, I., J.-L. Guerrero, J. Seibert, K. J. Beven, and S. Halldin (2011). “Stage-discharge uncertainty  
951 derived with a non-stationary rating curve in the Choluteca River, Honduras”. In: Hydrological Processes  
952 25.4, pp. 603–613. ISSN: 08856087. DOI: [10.1002/hyp.7848](https://doi.org/10.1002/hyp.7848).

953 Wilhelm, B., B. Amann, J. P. Corella, W. Rapuc, C. Giguet-Covex, B. Merz, and E. Støren (2022). “Recon-  
954 structing Paleoflood Occurrence and Magnitude from Lake Sediments”. In: Quaternary 5.1, p. 9. ISSN:  
955 2571-550X. DOI: [10.3390/quat5010009](https://doi.org/10.3390/quat5010009).